ABSTRACT

PONDE, AVINEET ARVIND. Finite Element Simulations of Interactions between Self-written Polymer Optical Waveguides. (Under the direction of Dr.Kara Peters).

This thesis presents a multi-physics, finite element model of the interactions between (1) two self-written waveguides at different input conditions and (2) a polymer element already present in the photosensitive UV- curable resin and a self-written waveguide in this resin. These models present the dynamics of the photopolymerization and lightwave self-focusing. A model of two UV laser beams being focused into the UV-curable resin was modeled using the commercial finite element code COMSOL. This model was then extrapolated to study the various interactions between waveguides written by these beams and with a polymer element in the resin.

The results obtained using these models were found to be in good agreement to experimental observations made by previous researchers. The interactions between two self-written waveguides in a particular resin system were studied for six different input approach angles: 30º, 17º, 15º, 12º, 9º and 5º. The presence of a critical angle of collision below which the waveguides merged and above which they crossed through one another was demonstrated numerically. In addition to these interactions the interactions between two waveguides formed by light beams with different input powers were simulated to check the concurrence of the computational model with the experimental observations. Further, the interactions between a thick polymer element at two different angles to the horizontal direction and a thin polymer element at an angle to the horizontal with a self-written waveguide were simulated. This thesis also provides a flexible computational model methodology for predicting different interaction scenarios in settings like resins and laser beams beyond those presented.

Finite Element Simulation of Interactions between Self-written Polymer Waveguides

by
Avineet A. Ponde

A thesis submitted to the Graduate Faculty of
North Carolina State University
in partial fulfillment of the
requirements for the degree of
Master of Science

Aerospace Engineering

Raleigh, North Carolina
2011

APPROVED BY:

Dr.Gracious Ngaile	Dr.Lawrence M.Silverberg

Dr.Kara J.Peters

Chair of advisory committee

DEDICATION

To my parents, family and my niece Sesha

BIOGRAPHY

The author was born in Mumbai, India and brought up in Pune, India. He has obtained a Bachelor's degree in Aeronautical Engineering from the Aeronautical Society of India, India. This is where he developed an interest for Aerodynamics and Aerospace Structures. After completing the undergraduate studies, the author worked as a project engineer at the National Aerospace Laboratories, Bangalore, India. He then joined the Department of Mechanical and Aerospace Engineering at North Carolina State University, Raleigh, NC, USA to pursue a Master's degree in Aerospace Engineering.

ACKNOWLEDGEMENTS

I would like to sincerely thank my adviser Dr.Kara Peters for her guidance, motivation, patience and support throughout these two years at NC State University. It was a nice learning experience working with Dr.Peters. I learnt the approach that one should have towards work from Dr.Peters. I am also thankful to Dr.Gracious Ngaile and Dr.Lawrence Silverberg for being on my advisory committee.

My special thanks to all my friends for making my stay at NC State enjoyable and memorable.

Finally, my deepest gratitude goes to my parents, my elder sister and my brother-in-law for their unending love and support.

TABLE OF CONTENTS

LIST OF TABLES

LIST OF FIGURES

Chapter 1 Introduction

1.1 Motivation

Spatial solitons, otherwise called self-trapped or self-guided light beams, are beams that do not spread as they propagate in an optical medium. This self-focusing occurs through a balance of beam expansion due to diffraction and a change in the refractive index of the material as the beam propagates. These solitons can be used for the fabrication of steerable, self-written waveguides that can guide other beams of different polarizations or wavelengths just like a standard optical fiber.

The fabrication of these self-induced or self-written waveguides requires the use of photosensitive materials, which undergo permanent refractive index changes in response to illumination at a specific wavelength. Multiple waveguides can be written in such photosensitive materials in the form of X- and Y-junctions to act as couplers [1]. Researchers have proposed to use these kinds of multiple waveguides as a self-reconfigurable waveguide circuit which offers potential advantages over traditional waveguide circuits [2]. Using this technology, one light-written structure can be erased and another one can be written to replace it [2].

These self-written waveguides can also be used as sensors. Recent work at North Carolina State University has demonstrated that self-repairing strain sensors can be formed between two optical fibers through self-writing [13]. Once the existing sensor is damaged, a new waveguide is written from the damaged one. There is a need to model the fabrication and strain response of these sensors such that (1) the sensors can be optimized for given applications; (2) their response to strain can be independently verified and (3) the effects of multiple repairs can be predicted. Numerical models based on axisymmetric geometries [19] and infinite domains have been previously developed for self-written waveguides [20]. Anderson and Peters [3] also constructed a multiphysics, axisymmetric, finite element model of self-writing that incorporates the effects of the changing waveguide geometry due to shrinkage of the photosensitive resin during cure. The goal of this thesis work is to extend this finite element model to a planar

geometry so that interactions between multiple waveguides can be accurately modeled and thus provide a tool to address needs (1) - (3) above.

1.2 Scope of Research

A finite element model of the self-writing process through photopolymerization was presented in [3]. The goal of this research is to incorporate more complex input conditions and a planar geometry which could simulate non axisymmetric self-writing phenomena. In particular, this model will simulate the collision process between two self-written waveguides and the collision of a self-written waveguide with a previously cured polymer element. Both cases are expected to occur during self-repair of the strain sensor of [13]. To verify the model performance, the interactions of waveguides formed by the two laser beams approaching at an angle to the horizontal are studied. Shoji *et al.* [1] experimentally demonstrated that for low collision angles the two waveguides merge to form a single waveguide whereas they pass through each other for angles above some threshold known as the critical angle. The effective waveguide then travels in the direction of the beam which has a higher power. Applying the finite element model created in this research, five cases are studied: (1) two beams approaching at a low angle (below the threshold value) to the horizontal; (2) two beams approaching at an angle close to the critical angle; (3) two beams approaching at an angle greater than the critical angle; (4) two beams with different powers colliding in the resin and (5) a self-writing waveguide, during its fabrication, interacting with an already present polymer element in the resin.

The outcomes of this research will also help future calibration of photo-sensitive resins with variable input parameters. The finite element model is implemented in COMSOL Multiphysics, a commercial code which would be readily available to researchers to utilize the code in the future.

1.3 Thesis Outline

Chapter 2 of this thesis reviews the field of self-written waveguides and their applications. Afterwards Chapter 2 presents previous numerical modeling to study the interactions of self-written waveguides.

Chapter 3 details the current finite element modeling of the self writing process and model chosen for the waveguide interaction and the interaction between a polymer element and

a self-writing waveguide. The Chapter 4 presents the results obtained from the model implemented into COMSOL Multiphysics and an interpretation of the results achieved. The goal of this chapter is to understand the previous experimental results and validate those results. Finally, Chapter 5 discusses the conclusions drawn from this research and recommends work to be carried out in future, specifically towards the development of novel self-written sensors for structural health monitoring of structures.

Chapter 2 Self-Written Waveguides

This chapter describes previous research done in the field of self-trapped beams and self-written waveguides. This review will develop the background required for understanding the current research.

2.1 Self-Written Polymer Waveguides

Recently self-guided (self-trapped) optical beams have been extensively studied. These beams propagate in slab waveguides or nonlinear bulk media without the need for supporting waveguide structures [6]. Such beams are known as spatial optical solitons. The innate tendency of optical beams is to diffract as they propagate in a homogeneous medium. However, this diffraction can be compensated for by beam refraction if the material refractive index is increased in the region of the incident beam under consideration. Some materials display considerable optical nonlinearity when their properties are temporarily modified by the propagating light beam. This kind of nonlinearity leads to self-trapping of the beam as it changes the refractive index of the medium in the region of the beam as shown in Figure 2.1. A self-trapped beam propagates unchanged without any external waveguiding structure.

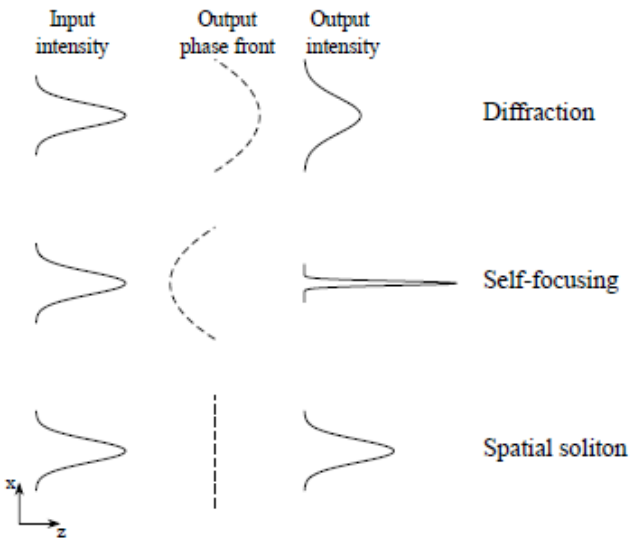

Figure 2.1 Qualitative picture of the beam self-trapping effect leading to the formation of a spatial optical soliton [6].

The optical solitons discussed previously have been studied extensively because of their possible use as steerable self-induced waveguides that can guide other beams of different polarization or wavelength. In order to permanently create soliton-induced waveguides, photosensitive materials have been used as they experience long-lasting refractive-index changes in response to illumination at a specific wavelength [7]. Photopolymerizable resins are made up of monomers and initiator molecules. When exposed to the UV light, the initiator molecules in the resin are excited to a higher state, causing the monomers to combine in order to form polymer chains in the resin material [4]. In the single-photon absorption (SPA) process, each initiator molecule absorbs a single photon. A similar process is the two-photon absorption (TPA) where the initiator molecules in the resin absorb two photons simultaneously [5]. The light absorbed by the TPA process is nonlinear in nature and the energy absorbed is proportional to the square of the incoming light intensity. In both cases, the polymer chains are formed only along the focal path of the light beam. This technique was also used by [18] to fabricate serially-grafted polymer waveguides where different materials are serially placed so that the waveguide core has different refractive index for different materials along its length. Also, the control of refractive index and hence the shape of the waveguides in was studied by [15].

The process of formation of such light-induced self-written waveguides from a standard optical fiber is shown in Figure 2.2. Firstly, the tip of the optical fiber is submerged in a

photopolymerizable resin bath. Lightwaves from the optical fiber expand into the resin in a Gaussian mode distribution and the resin begins to cure from the core of the optical fiber. Smaller waveguide structures can also be produced by focusing the lightwaves into the bath with a lens producing a converging input beam. The local rate of polymerization is proportional to the intensity of the lightwave. The core starts to grow longitudinally due to the self-trapping mechanism of the radiated beam in the polymerized core, as shown in Figure 2.2**Error! Reference source not found.**. Rapid growth proceeds ahead of the core tip until the radiative power is attenuated. As a result of this self-trapping, the process a straight, uniform-diameter waveguide through which light beams of different wavelengths can be propagated similar to traditional optical fibers [8]. This process of self-writing of waveguides, being a single-step process, provides greater flexibility in the creation of new waveguide structures as compared to waveguides fabricated by traditional techniques like ion exchange, plasma enhanced chemical vapor deposition (PECVD), flame hydrolysis deposition (FHD) and spin coating followed by reactive etching and/or photolithography including chemical processing. These traditional techniques are multistep, require more time and are expensive as compared to self-writing technique [9].

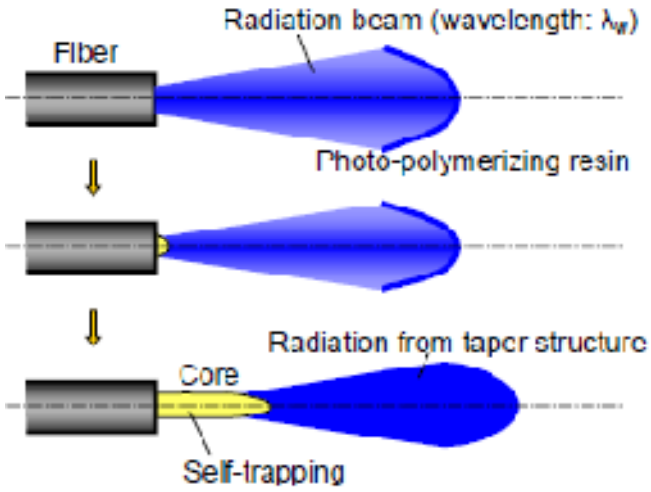

Figure 2.2 Light-induced self-written waveguide formation [8].

While theoretically, the self-writing process produces straight, uniform-diameter waveguides, the final output is extremely sensitive to the input conditions. For example, Dorkenoo *et al.* [14]

investigated the role of input power on the formation of multichannel and single channel waveguides inside photopolymerizable materials. Light was introduced in the resin (between two glass plates) through of a single mode optical fiber. It was observed that at a very low beam power of 5 μW, a unique uniform-channel waveguide without any broadening was formed by the photopolymerization process. As the input power was increased, the waveguide broadened and finally at a high input power of 100 μW, the waveguide became multichannel and eventually chaotic. These effects are shown in Figure 2.3 and are due to nonlinearities in the photopolymerization rate equation as a function of input optical power.

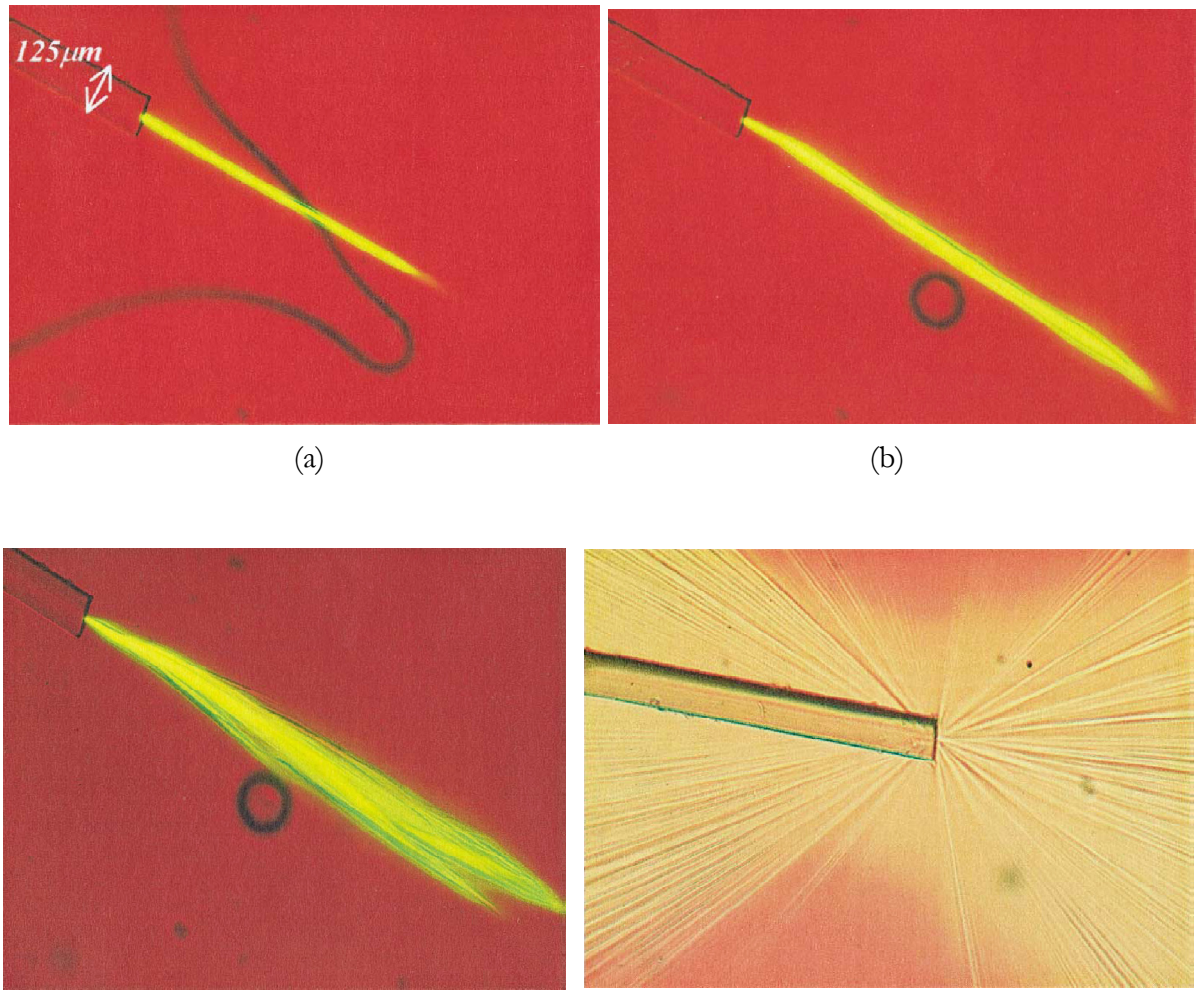

Figure 2.3 Self-writing waveguides created at different input powers. The waveguide becomes chaotic and multichanneled as power, P is increased. (a) P= 5 μW (b) P=8 μW (c) 16 μW (d) P= 100 μW [14].

2.2 Self-Written Polymer Strain Sensors

Huang *et al.* [10] fabricated hybrid silica/polymer optical fiber strain sensors using the self-writing fabrication process. Their goal was to fabricate optical fiber based strain sensors that could withstand a large strain range than conventional silica optical fiber based sensors. A polymer sensing element was fabricated between two silica fibers by the photopolymerization process discussed previously in 2.1 and by aligning the two fibers initially. One such sensor is shown in Figure 2.4. The applied strain was determined by measuring the shift of fringes in the

reflectance spectra of whitelight propagated through the silica optical fiber. The fringes were produced by reflections at the silica-polymer interfaces and are sensitive to the length of the polymer element. The polymer strain sensor was able to successfully measure strain up to 56% before failure, well above silica-based optical fiber sensors. Photographs of the sensor at different levels of deformation are shown in Figure 2.5. Although this type of sensors can measure high values of strains successfully, the length of such sensors is limited to 100μm because of high optical losses in these sensors [10].

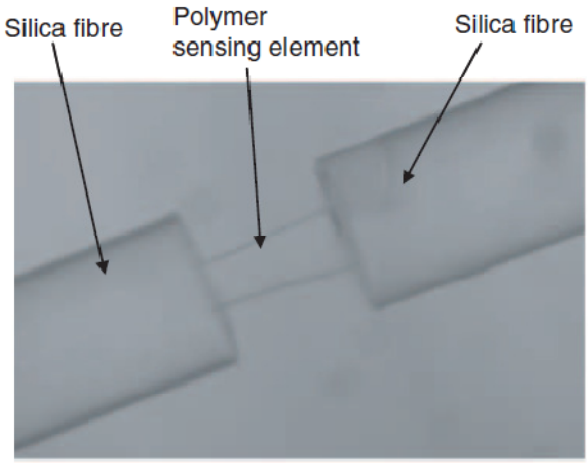

Figure 2.4 Microscopy image of hybrid silica/polymer strain sensor [10].

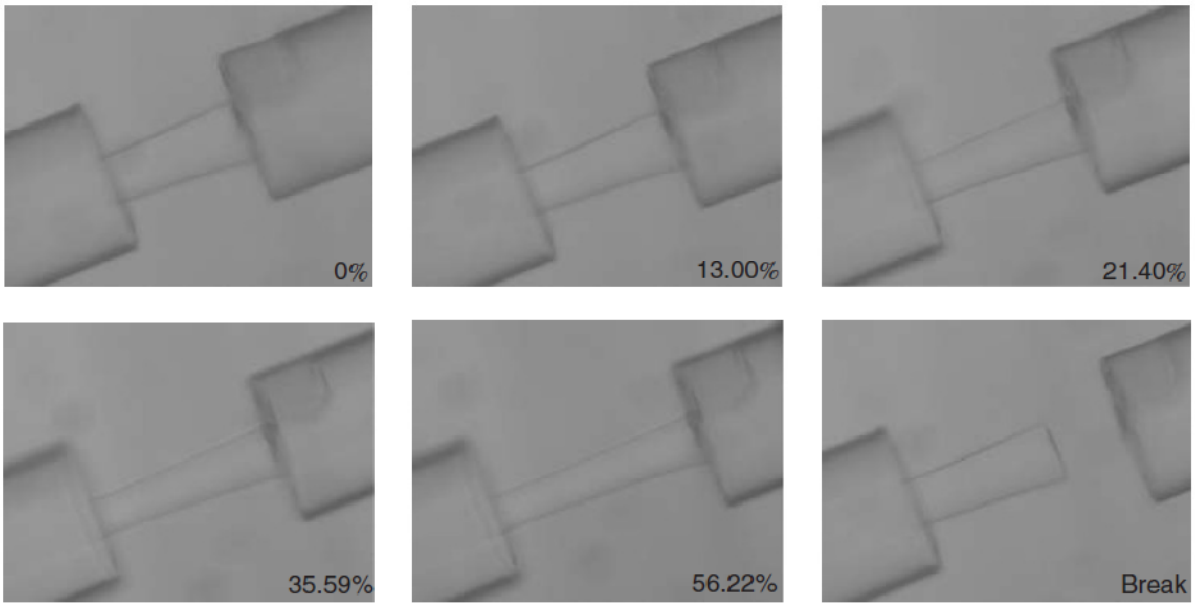

Figure 2.5 Micrographic images of the hybrid strain sensor at different strain levels [10].

This same fabrication process has been applied at North Carolina State University to create self-repairing sensors. A schematic of the self-repairing sensor system is shown in Figure 2.6. The sensor system consists of two polyimide sheets with optical fibers sensor packaged between these sheets and photopolymerizable resin surrounding the two optical fibers. A self-written waveguide was initially fabricated between the two optical fibers in the resin while the uncured resin still remains to repair any subsequent damage of the sensor. The applied strain is measured through the optical power loss of infrared lightwaves transmitted through the polymer waveguide. After the polymer waveguide sensor is damaged, the photopolymerization process will occur at the fractured locations of the sensor through UV illumination of the remaining resin to reconstruct the damaged waveguide sensor. To date, self-writing and self-repairing waveguides have been formed between two optical fibers and the self-writing process was optimized through the choice of optical fiber parameters, UV input power and gap length between the two fibers.

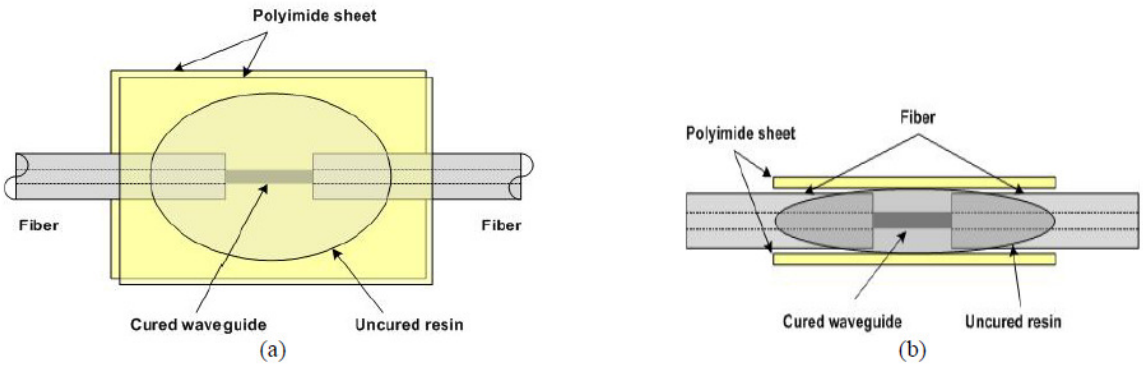

Figure 2.6 Schematic of proposed self-repairing optical fiber strain sensor: (a) top view and (b) side view [13].

The experimental setup for fabrication of self-writing waveguide at the end of a silica optical fiber is shown in Figure 2.7. Self-writing waveguides were repeatedly written between the two silica optical fibers [13]. The optical fibers were firstly aligned with a 500 μm gap between them. A UV laser with an excitation current of 30 mA and maximum output of 20mW was used to initiate photopolymerization. Waveguides were formed across the gap within one minute of the beginning of the process. Final images of waveguides between the two MM fibers are shown in Figure 2.8 for which the process was repeated five times using the same fibers under the same conditions. The previously formed waveguide and the uncured resin surrounding the waveguide were removed before each trial. The varying waveguide diameter is typical of waveguides written from the diverging beam exiting the optical fiber.

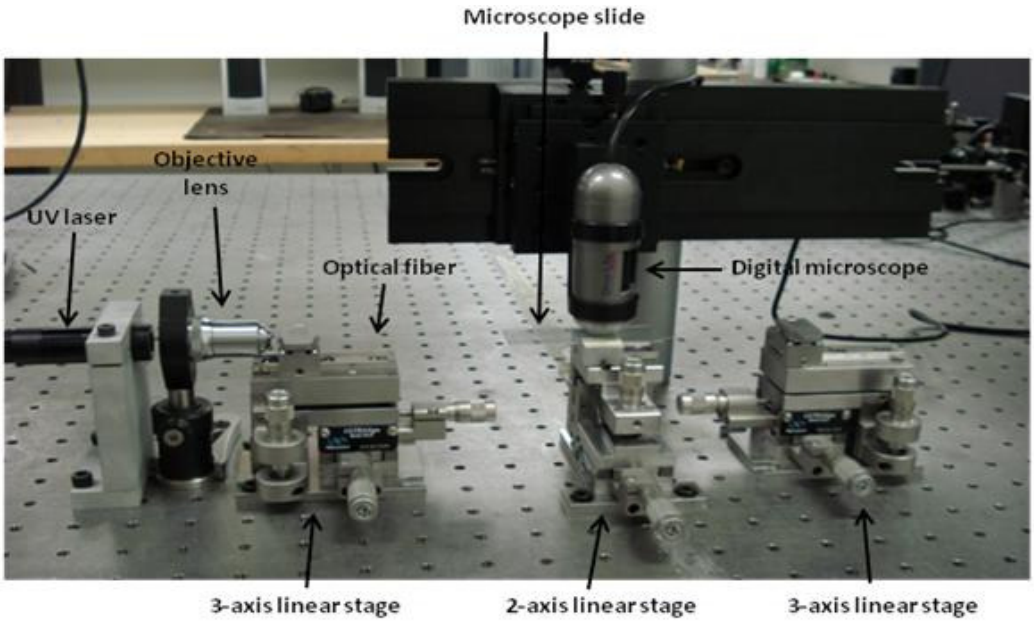

Figure 2.7 Experimental setup for self-writing waveguide fabrication at North Carolina State University [13].

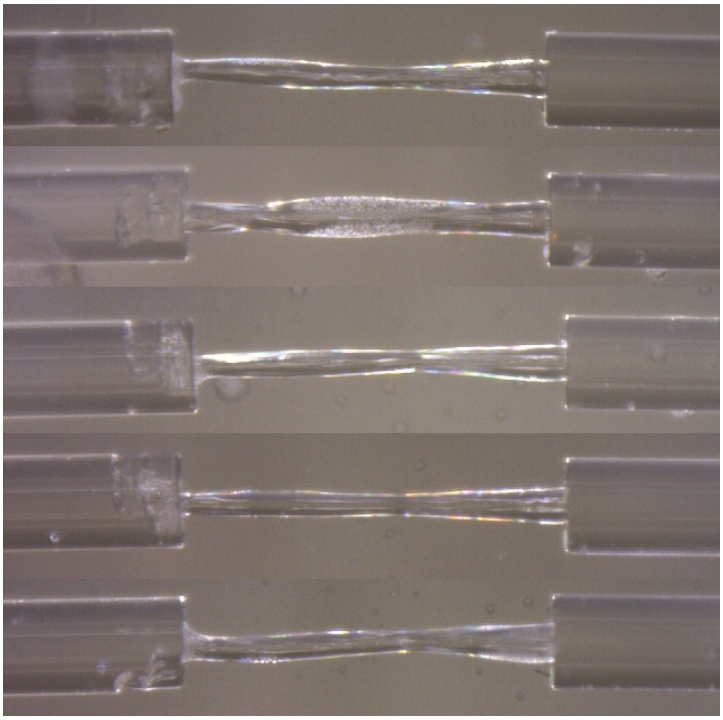

Figure 2.8 Microscopy images of final waveguide geometry for five different sensors across a 500 μm gap [13].

Later experiments demonstrated self-repair of the polymer waveguide. Figure 2.9 shows photographs of the senor during this process. The waveguide was originally written between the two optical fibers with a gap distance of 200 μm. This reduced gap distance produced a uniformly tapered sensor rather than the oscillating waveguide diameter observed earlier. After the waveguide was completed, tension was applied between the optical fibers until the sensor failed by disbanding from one of the polymer/silica interfaces. At this point, the UV illumination was repeated and the waveguide formed from the existing polymer waveguide, crossed the remaining gap and rebonded with the second silica fiber. The strain response of this repaired sensor was similar to that of the original polymer waveguide.

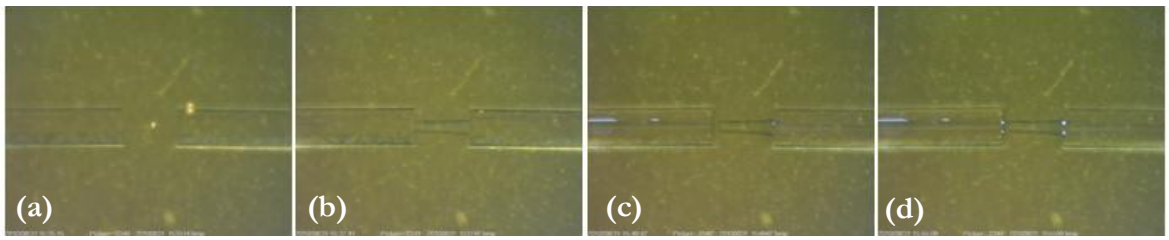

Figure 2.9 Microroscopy images of self-written waveguide (a) before fabrication; (b) after fabrication; (c) after failure and (d) after self-repair (Photographs courtesy of Young Song).

2.3 Self-Focusing Soliton/Waveguide Interactions

Johansen *et al.* [11] numerically investigated the interactions of solitons or self-trapped beams in a nonlinear medium, which is a medium in which the refractive index increases with the intensity of the electric field of the light which is focused into it. They found that complex waveguide structures can be generated by soliton interaction. They theoretically confirmed the existence of a critical angle between solitons approaching at angle. They referred to this critical angle as the "escape angle." This angle also depended upon the power transmitted by the solitons. For solitons approaching above this critical angle the solitons collided with diffraction of the solitons after the collision as shown in Figure 2.10(a). The final result was highly sensitive to the soliton power, and in some cases the interaction of the solitons resulted in annihilation as shown in Figure 2.10(b) [11].

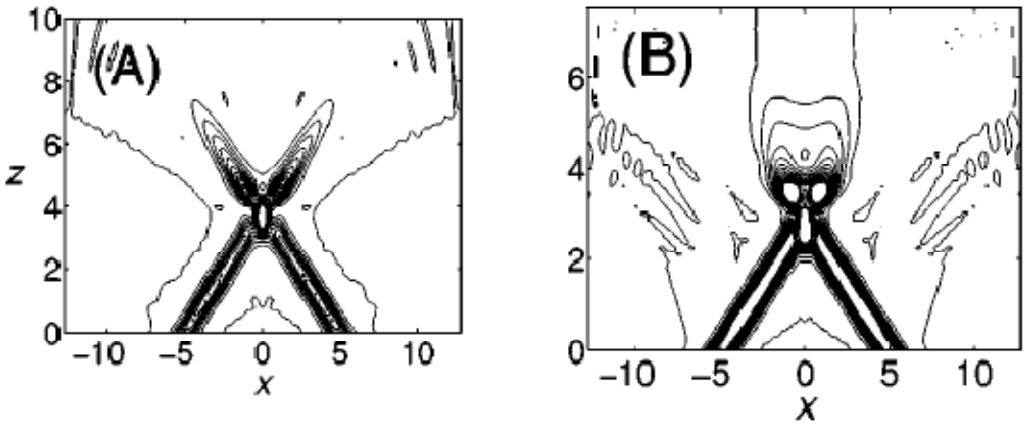

Figure 2.10 Predicted interaction of solitons: (a) Crossing followed by diffraction; (b) annihilation. [11]

The interactions between two solitons were also studied computationally by Kivshar *et al.* [16] including when the two solitons interact at a boundary between materials with different indices of refraction. In this case the solitons are called surface solitons. . They found that the outcome of collisions between these solitons strongly depends on parameters such as the distance of the centers of the solitons from the surface and their transverse velocities. They studied scenarios like soliton fusion, symmetric scattering and asymmetric collisions.

In the present research, various interaction scenarios between two self-writing waveguides and the interaction between a polymer element in the resin and a self-writing waveguide are simulated, as opposed to the interaction scenarios between just the solitons (self-trapped beams) studied in [11] and [16]. Shoji *et al.* [1] studied the interaction of self-written waveguides in a photosensitive material experimentally and found out that the waveguides behave in the same way after interaction as the solitons or self-trapped beams. They varied different parameters like collision angles, the time delay and power of the two beams during their experiment. They focused the two beams into a photosensitive resin (PR) such that the waveguides formed by the two beams interact in the PR at some angle to each other. The interactions that they observed are shown in Figure 2.11.

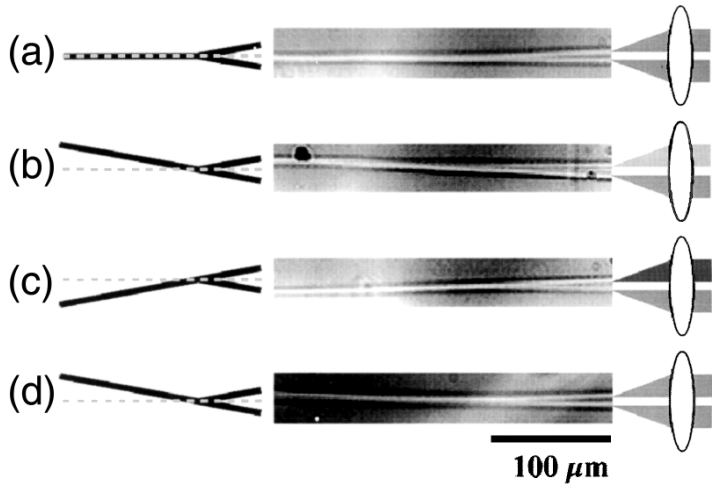

Figure 2.11 Microscopy images of collisions between two self-written waveguides. The lightwave is propagating from right to left. Schematic of final geometry is shown on the left-hand side. The power of the lower beam is 0.1 mW; the power of the upper beam is (a), (d) 0.1 mW, (b) 0.07 mW, and (c) 0.13 mW. The time delay between the lower and upper beams is (a)-(c) 0 s, and (d) 2 s [1].

They found that the waveguide formed after collision propagated in the direction of the beam which has higher power or was launched first into the photopolymerizable resin. Another effect that they studied was that the two waveguides merge to form a single waveguide only if they collide at some angle less than the critical value which is a characteristic of the beam and photopolymerizable resin used. For the photopolymerizable resin that they used, the critical angle was found to be 9º and the above results were obtained at an angle of 6.4º. If the beams collide at a higher angle than the critical angle, then the two waveguides just cross each other and this phenomenon can be used to fabricate an X-junction in an optical circuit. The merging of the waveguides can be used to form Y-couplers in optical circuits. One important thing to be noted is that the beams are focused in the resin using a lens whereas in the current research, the beams are modeled to be coming out of optical fibers. Hence more diffraction of the incident light can be anticipated in the current work.

2.4 Previous Theoretical Modeling

The first studies of self-focusing through photopolymerization were performed by Monro *et al.* [19], [20]. They applied a modal decomposition method to describe wave propagation through dynamically varying waveguides. The modal decomposition method is

advantageous because decomposing the electric field into modes reduces the complexity of the problem, as only the variation of modal coefficients need be calculated. In their first paper, Monro *et al.* [19] derived a two dimensional theory using this decomposition method to study the interactions of an electromagnetic field and the photosensitive glasses. In the second paper, Monro *et al.* [20] extrapolated the first work to three-dimensional geometries using a series expansion technique. Both works assumed axisymmetric geometries.

After this original work, several researchers continued the simulation of this process to include photopolymerizable resins, non-linearities with respect to optical power and oxygen diffusion into the resin. Hocine *et al.* first applied the finite element method to model microtips formed at the end of an optical fiber [23]. The advantages to the finite element method for these simulations are that complex input conditions can be modeled. Similar to the decomposition method, the propagating modes do not need to be known at the beginning of the simulation.

As described in the previous section, Johansen et al. [11] modeled the interaction of propagating solitons (not self-written waveguides) as they propagated through a medium. Their simulation was based on soliton solutions to the paraxial wave equations (the same equation previously used by [19], [20]). The interaction between the two waveguides was then included assuming a weak interaction between the two solitons. This weak interaction assumption is not valid in the region where the solitons actually overlap, therefore the authors clarify that the results in this immediate interaction region (see Figure 2.10 (a) and (b)) are not correct. As the goal of these simulations was to predict the critical angle for the soliton interaction, however, the model was still applicable. When predicting the final geometry of interacting polymerized waveguides, this region will also be an issue, as will demonstrated later in the results of this thesis.

Anderson and Peters [3] applied the finite element method to model the polymerization rate equation, mechanical shrinkage (density changes) and lightwave propagation through the waveguide during the self-writing process. The mechanical shrinkage is important for photopolymerizable resins, as compared to photosensitive glasses which do not significantly deform during the process, and was introduced through an effective body force. A single waveguide was modeled starting from an optical fiber. The model geometry with the

electromagnetic and mechanical boundary conditions to be incorporated in COMSOL is shown in Figure 2.12 The development of the waveguide in the resin and the mechanical shrinkage effect is shown in Figure 2.13. Three stages of the self-writing process were observed: (1) a relatively slow beginning of the polymerization process (t=1 to 4 s); (2) a rapid increase in the Δn due to large number of polymer chains being excited as the light waves are focused (t= 5 to 14 s) and (3) saturation stage where the polymerized structure stabilizes (t= 15 to 50 s) [3]. More detail on this model will be provided in the Chapter 3.

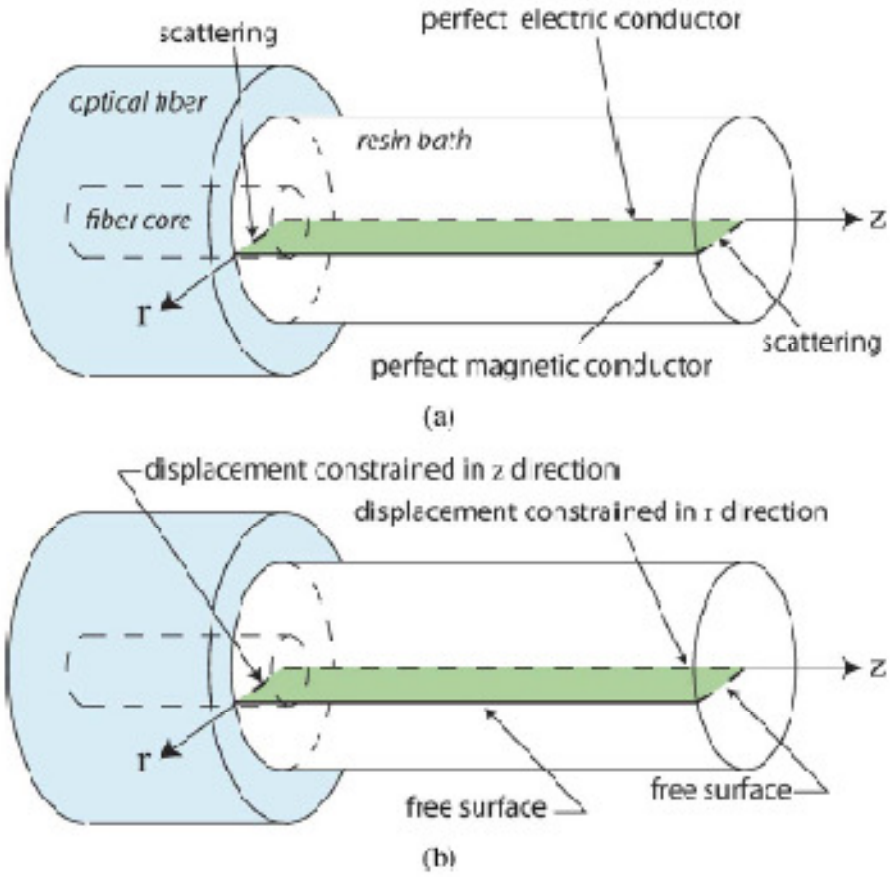

Figure 2.12 Model geometry with (a) electromagnetic and (b) mechanical boundary conditions

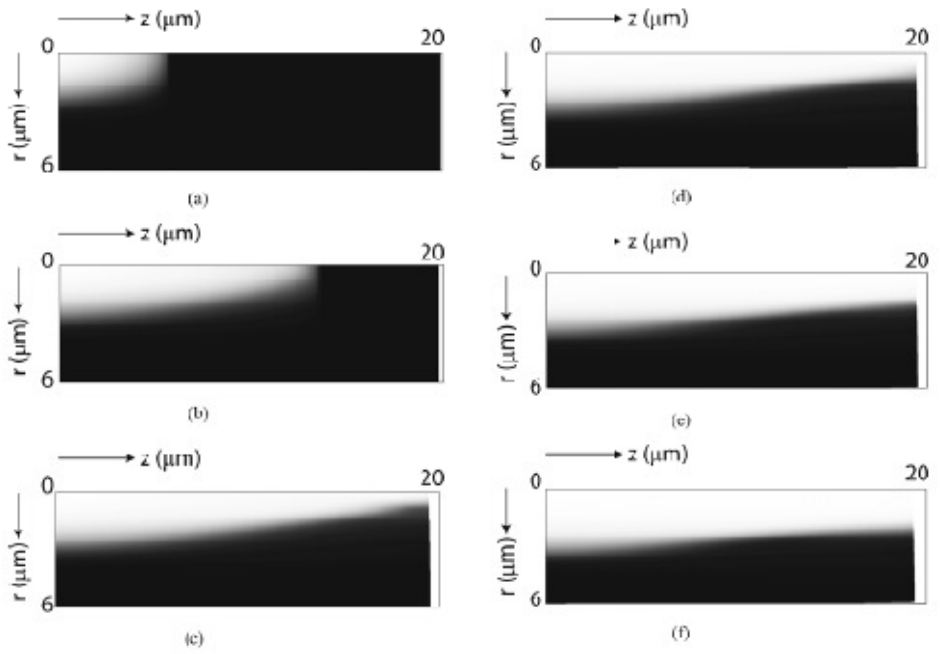

Figure 2.13 Greyscale plot of index of refraction, *n*, distribution including mechanical shrinkage at various time steps. Black and white limits correspond to *n*=1.482 and *n*=1.52 respectively. Deformation of original resin volume is also shown to scale. (a) t= 3s (b) t= 7s (c) t= 12s (d) t=17s (e) t= 25s (f) t= 50s [3], [4].

2.5 Goals of This Research

The main goal of this research is to computationally simulate the interaction between two waveguides which was previously observed by [1] experimentally. Further, the interaction between a polymer element already present in the resin and a self-writing waveguide will be simulated using. These simulations will be generated by expanding the previous finite element model of Anderson and Peters [3]. These computational models would allow future researchers to optimize the design of self-written waveguides without the need for a large number of experiments in the laboratory. The study of waveguide interactions was specifically chosen because the self-repairing waveguide sensor of [13] is expected to experience such situations during repair. Five cases will be studied: (1) two beams approaching at a low angle (below the threshold value) to the horizontal; (2) two beams approaching at an angle close to the critical angle; (3) two beams approaching at an angle greater than the critical angle; (4) two beams with different powers colliding in the resin and (5) a self-writing waveguide, during its fabrication,

interacting with an already present polymer element in the resin. The computational model for this research will be implemented into COMSOL, a commercially available finite element code. This would provide easy use of the code to other researchers.

The next chapter discusses the numerical modeling of the interactions of waveguides and between a polymer element in the resin and a self-writing waveguide based on electromagnetic and chemical process required for photopolymerization.

Chapter 3 Numerical Modeling

The main goal of this chapter is to describe the methodology behind the finite element model to study the interaction of self-writing waveguides. This model is based on coupling of the two physical phenomena of electromagnetic wave propagation and chemical reactions (polymerization). This chapter also provides the analytical background required to model the process of interacting waveguides and interactions between a polymer element present in the resin and the self-writing waveguide. The model created in COMSOL can be easily replicated in a laboratory and could allow for the calibration of resins on the basis of: (1) the time required for photopolymerization and (2) the critical collision angle of the two beams for interactions between two waveguides. This experimental calibration is not considered in this thesis.

In order to replicate the experimental work currently in progress at North Carolina State University, described in Section 2.2, the input parameters are chosen to match the UV Laser (output wavelength, λ=375 nm) and the UV curable epoxy resin applied.

The sample cell modeled was a rectangular resin bath to match the experimental arrangement. Although the actual arrangement is not two-dimensional, a two-dimensional model of the system was created. This two-dimensional reduction in the model was required due to the high mesh density and small time steps that were required. The effects of this two-dimensional assumption will be discussed in the next chapter. Such an approach was also applied by previous researchers for the same reasons [11].

The parameters that were chosen to match the experimental setup include the initial index of refraction of the uncured polymer (n_0), the index of refraction for the fully cured resin (n_{max}), the wavelength of the input laser beam (λ_0), the amplitude of the input laser beam (E_0), and the waist of the Gaussian mode distribution of the lightwave exiting the optical fiber (w_0).The wave number ($k_0 = 2\pi/\lambda$) was also calculated from these input parameters.

The steps involved in the computational modeling of the photopolymerization process have been summarized with the help of a flowchart shown in Figure 3.1. The independent variable defining the process at each point in the resin bath is the normalized polymer

concentration, $\tilde{P}(x,y,t)$. $\tilde{P}(x,y,t)$ ranges from 0 (unpolymerized resin) to 1 (completely polymerized resin) and is related to the local index of refraction through

$$\tilde{P}(x,y,t) = \frac{n(x,y,t) - n_0}{n_{\max} - n_0} \tag{3.1}$$

The resin bath initially has a uniform refractive index initially given by $n\,(x,y,0) = n_0$ and normalized polymer concentration $\tilde{P}(x,y,0) = 0$. The electric (**E**) and magnetic (**H**) are evaluated for each time step which are then used to compute the power flow ($\mathbf{S}_x$) in the x-direction and hence the intensity ($\mathbf{I}_x$). The intensity is the driving force for photopolymerization as it excites the monomers in the resin bath to form polymer chains. It is linearly related to the power flow. The change in the polymerization state $\Delta\tilde{P}(x,y,t)$ is then computed. The index of refraction of the resin is then updated for each time step based on this value of the change in polymerization state and updated.

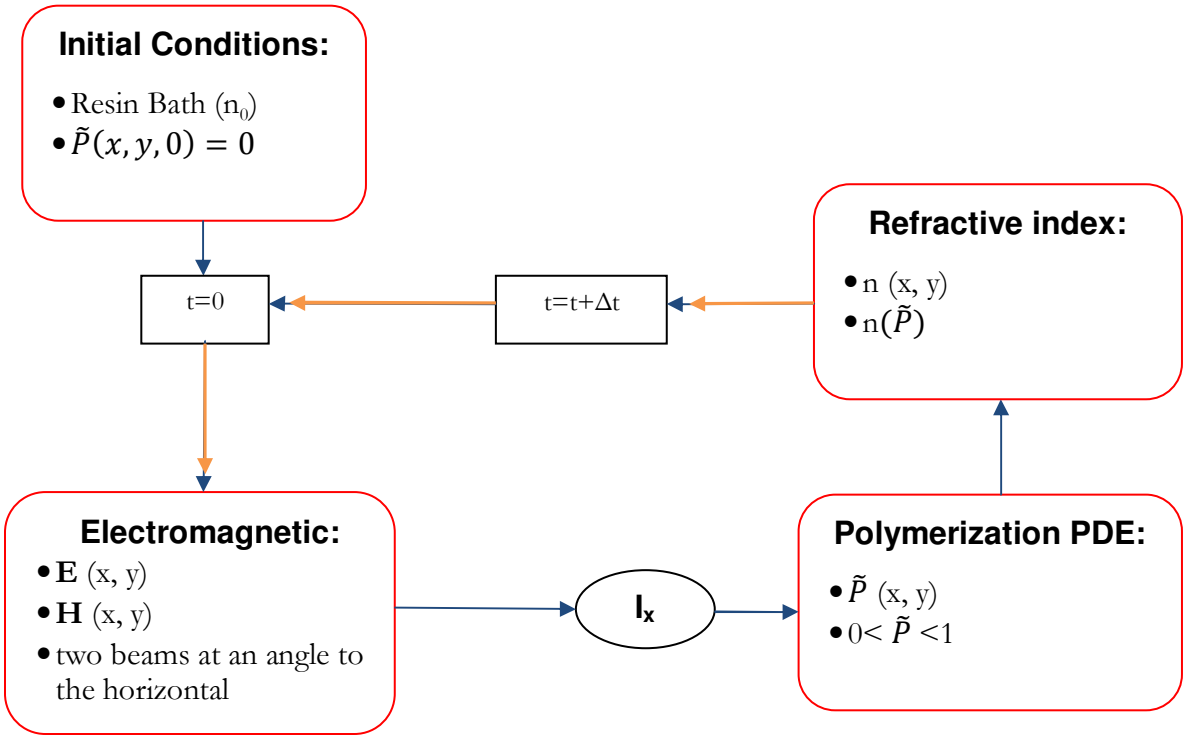

Figure 3.1 Outline of the computational modeling process (a) Electromagnetic beams focused in the resin at some angle to the horizontal (b) Increasing polymer concentration in the resin bath (c) Change in refractive index of the resin with time

3.1 The Domain

Two different computational domains were applied to model the interactions between two self-writing waveguides and between a polymer element in the resin and a self-writing waveguide.

3.1.1 Computational domain for interaction between two waveguides

The resin bath in the experimental setup is a cylinder with a radius of 12 μm and length 80 μm. Although the resin bath is radialy symmetric, the waveguide formation is not. However, the waveguide formation only occurs near the center of the resin bath. This sample volume was reduced to a two-dimensional area, a rectangle with a length of 80 μm and width of 24 μm as shown in Figure 3.2.

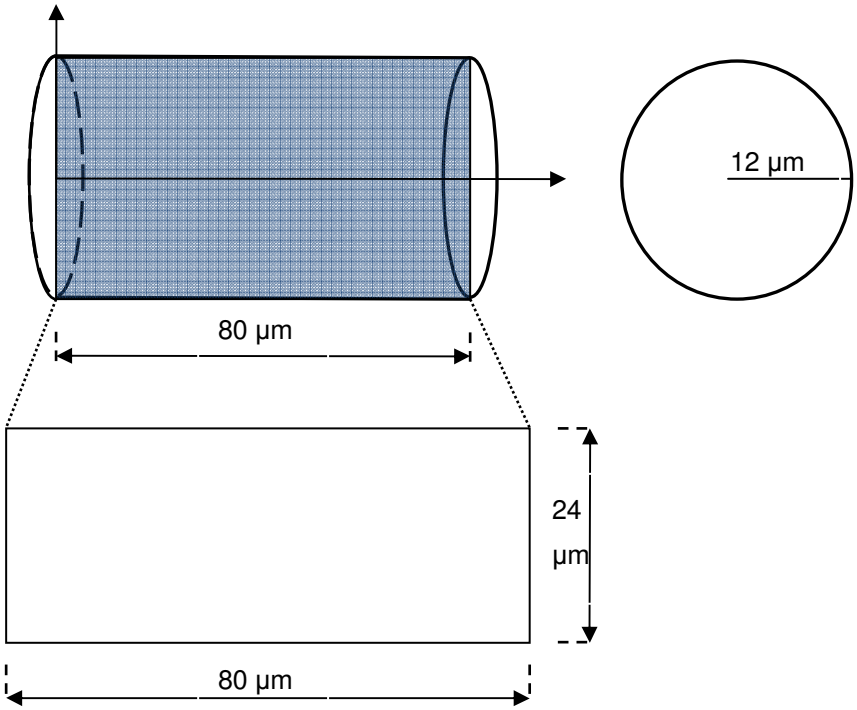

Figure 3.2 The domain for the computational modeling process of interactions between two self-writing waveguides.

3.1.2 Computational domain for interactions between polymer element in the resin and a self-writing waveguide

In this case, a similar resin bath with smaller dimensions was applied, a rectangle of 40 μm length and 24 μm width as shown in Figure 3.3. The smaller domain was necessary due to more computationally intensive mesh required of the finite element model of this problem.

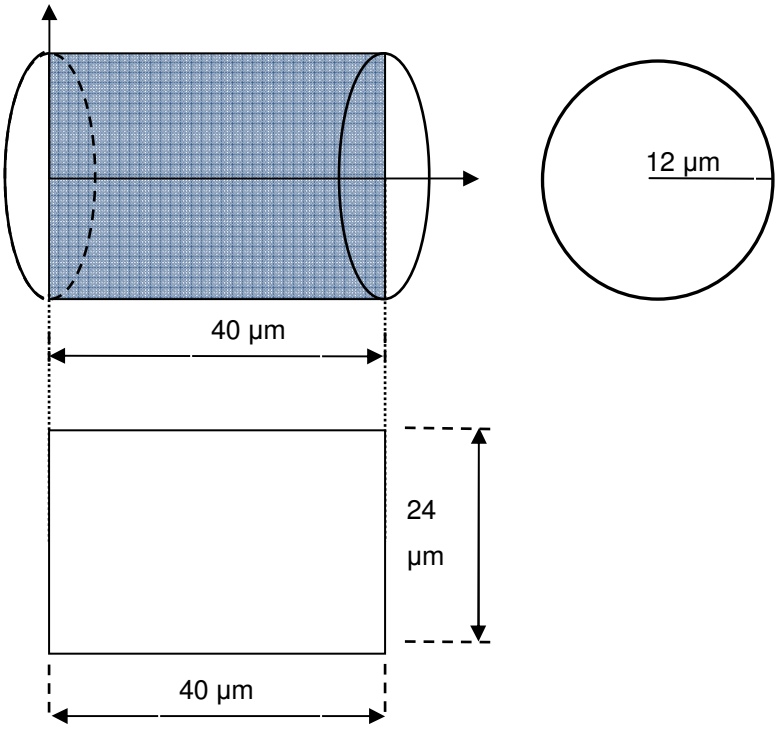

Figure 3.3 The domain under consideration for the computational modeling process of interactions between polymer element in the resin and a self-writing waveguide.

3.2 Electromagnetic Wave Propagation

The wave equations for the propagation through a medium are given by Maxwell's equations as,

$$\nabla \times \mathbf{E} = \mu_0 \frac{\partial \mathbf{H}}{\partial t} \tag{3.2}$$

$$\nabla \times \mathbf{H} = -\varepsilon_0 n(x,y,t)^2 \frac{\partial \mathbf{E}}{\partial t} \tag{3.3}$$

Where μ_0 is the permeability of the free vacuum ($\mu_0 = 4\pi \times 10^{-7}\, H/m$) and ε_0 is the permittivity of a vacuum ($\varepsilon_0 = 8.854 \times 10^{-12}\, F/m$). Since the index of refraction changes with space, the electric and magnetic fields cannot be decoupled and are both solved in the

model. The power flow of the incident light is given by the Poynting vector **S,** which is the cross product of electric and magnetic fields,

$$\mathbf{S} = \mathbf{E} \times \mathbf{H} \tag{3.4}$$

To define the initial conditions of the electromagnetic field for the domain we define a Gaussian input mode distribution for each input beam (to match the output profile of the optical fiber from which the lightwave is exiting). The amplitude of the electric and magnetic fields arriving at the left boundary of the domain shown in Figure 3.2 for a beam traveling in the x direction are defined by

$$E(x,y,z,t) = E_0\{e^{-\left(\frac{x^2+y^2}{w_0^2}\right)}\cos(\omega_0 t - k_0 x)\} \tag{3.5}$$

$$H(x,y,z,t) = H_0\{e^{-\left(\frac{x^2+y^2}{w_0^2}\right)}\cos(\omega_0 t - k_0 x)\} \tag{3.6}$$

E_0 is the peak electric field applied and ω_0 is the angular frequency of the wave.

In order to implement multiple input beams at directed in different propagation directions in COMSOL, the exterior boundary on the left hand side of the domain had to be split into two separate boundaries. The first of these boundaries is highlighted in red in Figure 3.4. In order to rotate the input beam to an arbitrary angle (θ) to the horizontal at boundary 1 (highlighted in red) shown in Figure 3.4 , co-ordinate transformations were applied as shown in equations (3.7) and (3.8).

$$x_1 = xcos(-\theta) - ysin(-\theta) - y_0 \tag{3.7}$$

$$y_1 = xsin(-\theta) + ycos(-\theta) - y_0 \tag{3.8}$$

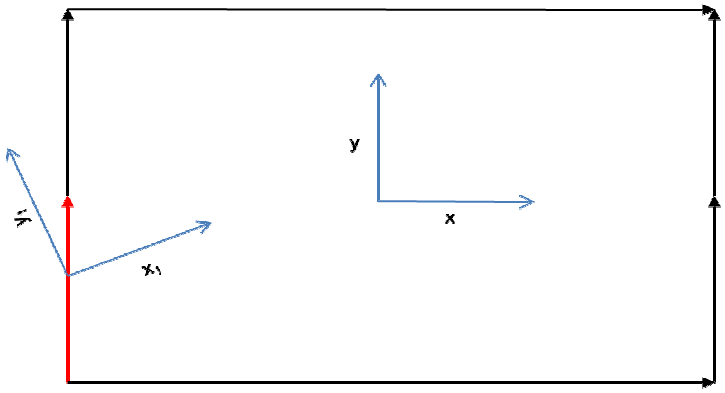

Figure 3.4 x-y and x_1-y_1 co-ordinate systems shown for boundary 1 of the domain.

Similarly, for boundary 2 (highlighted in red) shown in Figure 3.5, the co-ordinate transformation equations are as given in equations (3.9) and (3.10).

$$x_2 = xcos(\theta) - ysin(\theta) + y_0 \tag{3.9}$$

$$y_2 = xsin(\theta) + ycos(\theta) + y_0 \tag{3.10}$$

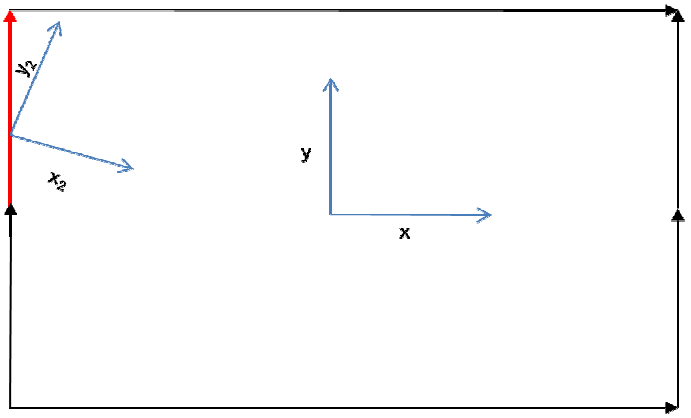

Figure 3.5 x-y and x_2-y_2 co-ordinate systems shown for boundary 2 of the domain.

Hence for boundary 1, substituting transformations (3.7) and (3.8) into equation (3.5) we get the equation of the beam at an angle of (-θ) to the horizontal as,

$$E_{bnd1} = E_0 \left\{ e^{-\left(\frac{{x_1}^2+(y_0+y_1)^2}{w_0^2}\right)} \cos(\omega_0 t - k_0 x_1) \right\} \tag{3.11}$$

Where the term y_0 gives the location of the beam axis intersecting the boundary under consideration. Similarly for boundary 2, substituting transformations (3.9) and (3.10) in equation (3.5) we get the equation of the beam coming in at an angle (θ) to the horizontal as,

$$E_{bnd2} = E_0 \left\{ e^{-\left(\frac{{x_2}^2+(-y_0+y_2)^2}{w_0^2}\right)} \cos(\omega_0 t - k_0 x_2) \right\} \tag{3.12}$$

A scattering boundary condition was applied in COMSOL for boundaries 1 and 2 the input electric field amplitude given by equations (3.11) and (3.12) respectively. For all other boundaries, a scattering boundary condition with zero input was applied. For the model of the interactions between a polymer element and a self-writing waveguide, the input lightwave was propagating along the x-axis and the scattering boundary condition was given as,

$$E_{bnd} = E_0 \left\{ e^{-\left(\frac{x^2+y^2}{w_0^2}\right)} \cos(\omega_0 t - k_0 x) \right\} \tag{3.13}$$

The electromagnetic and chemical reactions during the photopolymerization process occur on exceedingly different time scales which poses a challenge to compute properties like the lightwave intensity and the refractive index change over time. In order to accurately compute the propagation of the wave and the waveguide, the time steps have to be on the order of the period of the lightwave to prevent the numerical attenuation of the beam. Hence it was found that a time step of 2×10^{-17} seconds was required and the simulation was run for 20×10^{-14} seconds so that the two beams interact and the effective waveguide or waveguides propagate. Additionally, the mesh size must be small as well.

It is not reasonable to compute such small steps throughout the full length of time it takes to complete the polymerization process, which is on the order of seconds. The polymerization reaction is linearly related to the intensity of the lightwave, which can only be

determined by averaging the electric field over one period (125×10^{-17} s) in this model. Thus 63 time steps should be calculated before the photopolymerization reaction is calculated. Using the assumption that polymerization occurs very slowly as compared to electromagnetic propagation (and the electric field amplitude is periodic with time as long as the polymerization is constant), Anderson and Peters [3] updated the photopolymerization reaction directly from the instantaneous power flow and not the time average intensity. At each time step there is an error in the calculation, however the net error over several periods was shown to be negligible. This assumption is valid when rapid changes in the photopolymerization state do not occur. The effects of this assumption in the region when the two waveguide interact will be evaluated in the results of the next chapter.

3.3 Photo-polymerization

In order to account for both polymerization as well as electromagnetic wave propagation, the rate equation has to be scaled down to the time scale of the electromagnetic wave propagation. A new, normalized time variable, t, was therefore defined as

$$\tilde{t} = t/\beta \tag{3.14}$$

where β was chosen to be 1 x 10^{-14} s for these simulations. The global time t was divided into time steps Δt in the flowchart given in Figure 3.1. However, the polymerization rate equation, which we will discuss shortly, depends on the local polymerization state throughout the resin. For this reason, we need to define a "local time" to evaluate the rate equation at each point in the resin, $s(x, y)$ [3]. This local time variable is a function of the polymerization state and is updated for each time step as well. Figure 3.6 and Figure 3.7 [4] show the illustration of inclusion of the variable s in the computations. In Figure 3.6, the polymerization states at points 'a' and 'b' are different where the polymer concentration at point 'a' which is near the propagation axis of the light, is higher than that at point 'b' which is farther away from the propagation axis of the light. These two points are shown to fall on the plot of polymerization state as a function of $s(x, y)$ in Figure 3.7.

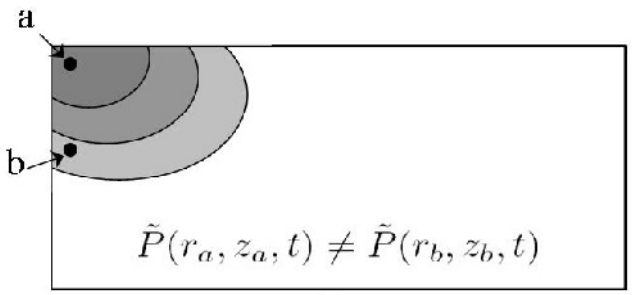

Figure 3.6 Polymerization state at time *t* [4].

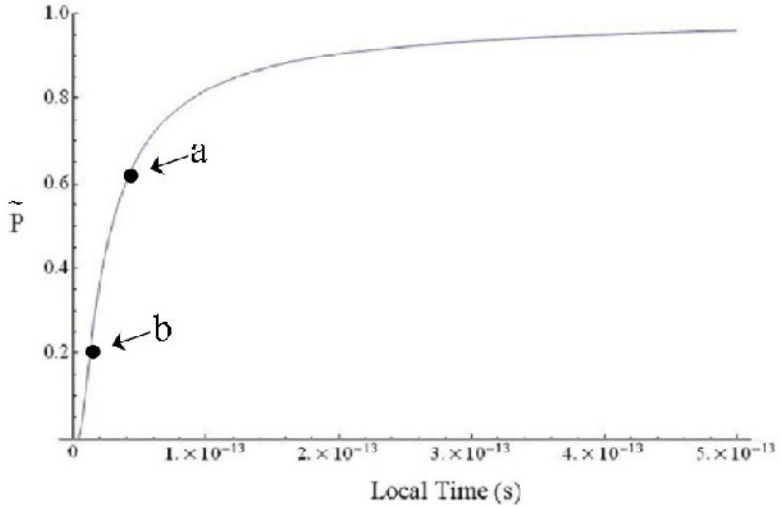

Figure 3.7 Polymer concentration curve showing spatial dependence [4].

An empirical polymerization concentration equation which demonstrates saturation was proposed in [4] and is applied in this work,

$$\tilde{P}(s) = e^{(-\frac{\beta}{s})} \tag{3.15}$$

This concentration equation gives the photopolymerization rate equation as

$$\frac{d\tilde{P}}{ds} = (\frac{\beta}{s^2})e^{(-\frac{\beta}{s})} \tag{3.16}$$

Additionally, the local time can be calculated from any photopolymerization state as,

$$s(x, y) = -\beta/\ln[\tilde{P}(x, y)]$$

This simplified equation is used as a footing for defining the change in refractive index in relation to polymerization. Initially the refractive index of the completely uncured resin is n_0 and it changes with every time step by an amount Δn. Hence for this transient process the refractive index has to be updated for each time step as,

$$n_t = n_{t-1} + \Delta n_t \tag{3.17}$$

The change in index of refraction is related to the polymerization equation as,

$$\Delta n(x, y, t) = \alpha S_x(x, y, t) \frac{d\tilde{P}(x, y, t)}{dt} \Delta t \tag{3.18}$$

The coefficient α is related to the properties of the resin. From the simplified polymerization concentration equation (3.15), the rate equation (3.16) is derived, which we can substitute equation (3.16) in equation (3.18). Hence the final algebraic equation for the change in the refractive index, which can be incorporated in COMSOL becomes,

$$\Delta n(x, y, t) = \alpha S_x(x, y, t) \left(\frac{\beta}{s^2}\right) e^{\left(-\frac{\beta}{s}\right)} \Delta t \tag{3.19}$$

Now that we have developed the numerical model of the photopolymerization process, we will proceed to explain the cases studied in this research. Firstly, the interaction between two self-writing waveguides arriving at some angle to the horizontal axis and at different input powers will be studied. Secondly, the interaction between a polymer element already present in the resin bath and a self-writing waveguide in the resin will be studied.

3.3.1 Case I: Interaction between two self-written waveguides in the resin bath

The lightwaves exiting the optical fibers enter the resin bath at some fixed angle θ as shown in the figure below. The various angles used to simulate the interaction process in COMSOL are a) 30º, b) 17º, c) 15º, d) 12º, e) 9º and f) 5º. In addition to these input conditions, the interactions for input beams with different powers has been simulated with the power of the upper beam being 50 per cent that of the lower beam.

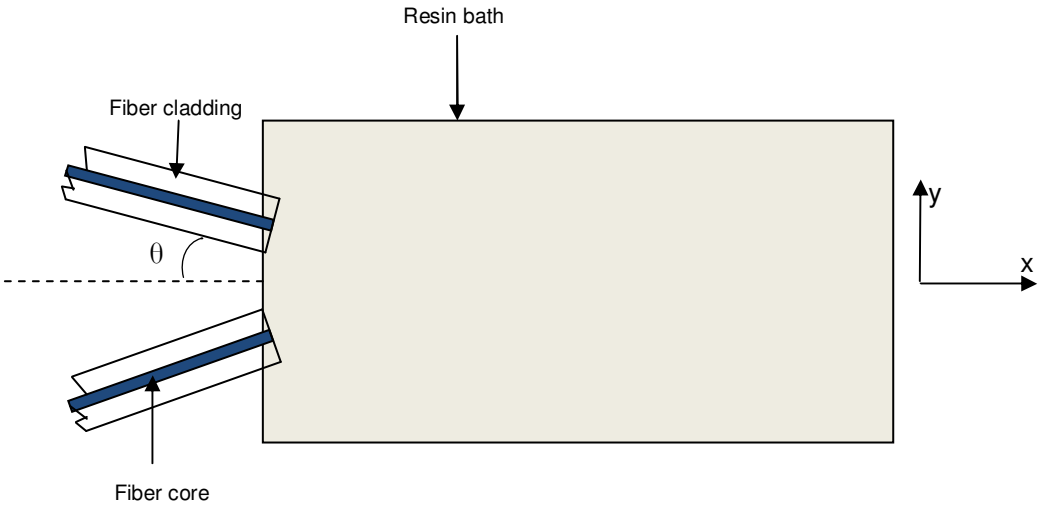

Figure 3.8 Schematic of the model used for interaction of two self-writing waveguides in the resin bath.

3.3.2 Case II: Interaction between a rotated polymer element present in the resin bath and a self-written waveguide in the resin bath

Here the ligthwave from just one optical fiber is considered as the interaction between a polymer element at some angle already present in the resin bath is to be simulated using COMSOL. The polymer element is assumed to be full cured, i.e. $n = n_{max}$. The optical fiber is aligned to the x-axis and the polymer element is in the path of waveguide that is to be written at an orientation θ. The schematic of this model is shown in Figure 3.9.

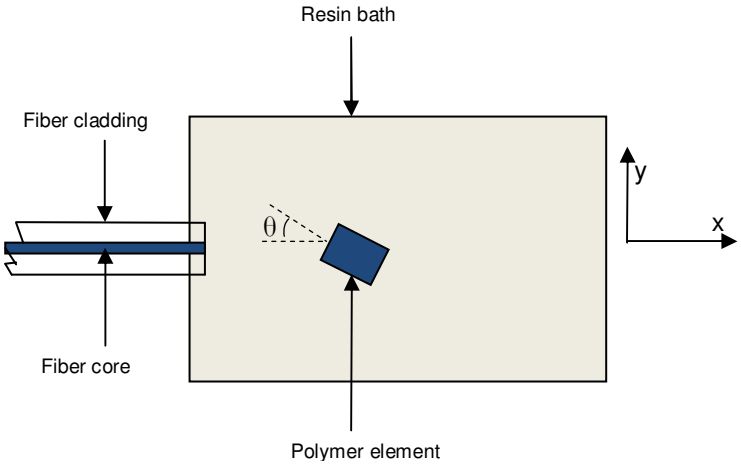

Figure 3.9 Schematic of the model used for interaction between a polymer element and a self-written waveguide in the resin bath.

Chapter 4 Results and Discussion

4.1 Interactions of two inclined self-writing waveguides

Prior to studying the interactions of two waveguides, the first challenge was to incorporate the correct input conditions and modeling domain. As discussed in section 3.3, the right value of the time scale constant β had to be found in order to correctly approximate the polymerization equation given by (3.16). This time scale adjustment had already been applied by [3], therefore the same scaling β was applied. The second input condition that needed to be modeled correctly was the ratio of the lightwave input power density to the photo-polymerization reaction constant α. The input power density is a function of E_0 and w_0 for the input beam. While the beam waist output from the optical fiber was known for the experimental conditions, the lightwave amplitude and α were not known. These parameters were adjusted until the correct behavior was observed in the finite element model. With these correct input conditions and co-ordinate transformations, two distinct waveguides of the right waist size and refractive index distribution were obtained as shown in Figure 4.1.

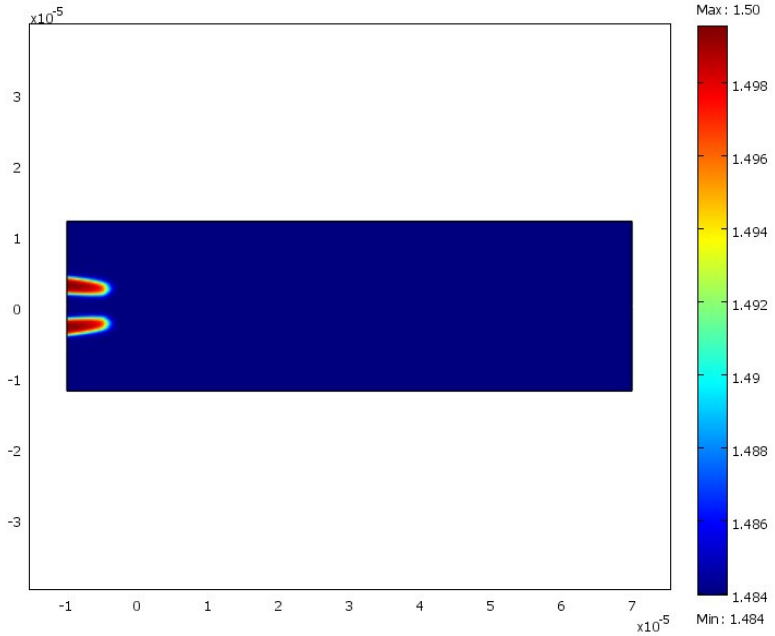

Figure 4.1 Refractive index surface plot for final boundary and input conditions.

In contrast, the refractive index contour plot for incorrect boundary conditions is shown in Figure 4.2. It can be seen that the waveguides are not confined and the refractive index distributions are not realistic. The refractive index gradients spread over a larger area in the domain which was not observed experimentally for the waveguides in the domain.

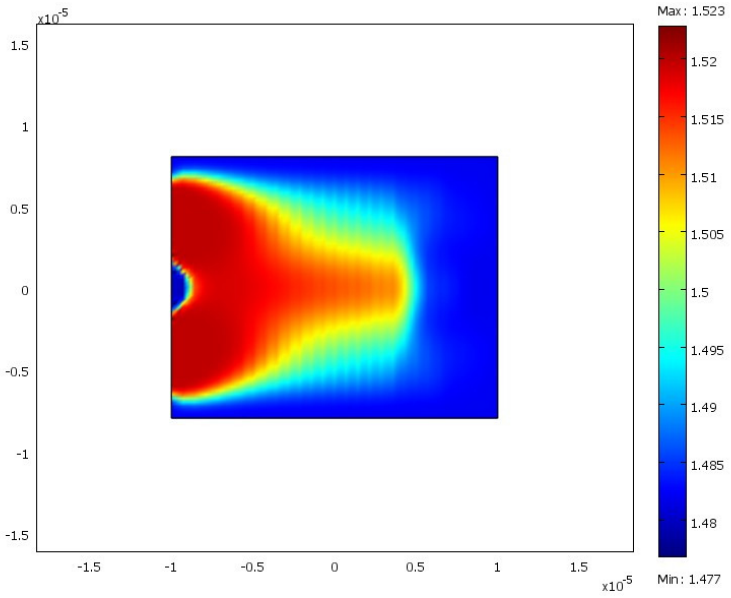

Figure 4.2 Refractive index surface plot for incorrect boundary and input conditions.

The third condition that had to be correctly included was the mesh size. Choosing elements that were too large did not accurately simulate the lightwave propagation. For this case, reflections were observed off the input boundary and the lightwave did not fully propagate into the resin bath. In order to achieve acceptable results, the domain was meshed with 40,000 quadrilateral elements. The final selection of appropriate parameters used to model the interactions between two waveguides in the resin bath are given in Table 4.1.

Table 4.1 Parameters used in finite element model.

Variable	Value	Units
λ	375×10^{-9}	m
w_0	1×10^{-6}	m
E_0	3×10^{15}	V/m
n_0	1.482	-
n_{max}	1.50	-
α	1×10^{-7}	m^2/W
β	1×10^{-14}	s

The following section will present the results obtained for the interactions between waveguides written in the resin at various angles to each other. We start with an angle of 30º, chosen because it would be well above the critical angle, then reduce the angle down to 5º. A simulation where the power of the upper beam is half that of the lower beam was also run for beams arriving at an angle of 9º to the horizontal axis.

4.1.1 Waveguides at 30º input angle to the horizontal

It can be seen in figures (a)-(f) in that the two beams come in at angle of 30º to the horizontal and the waveguides formed by these two beams interact inside the resin. The two-dimensional finite element model represents the time-dependent self-writing process well. It can further be seen that the beams cross each other and continue to fabricate in the same direction rather than merging to form a third waveguide along the bisection angle of the two waveguides. The interaction did not significantly affect the propagation of either waveguide.

Figure 4.3 Refractive index change for beams at 30º input angle.

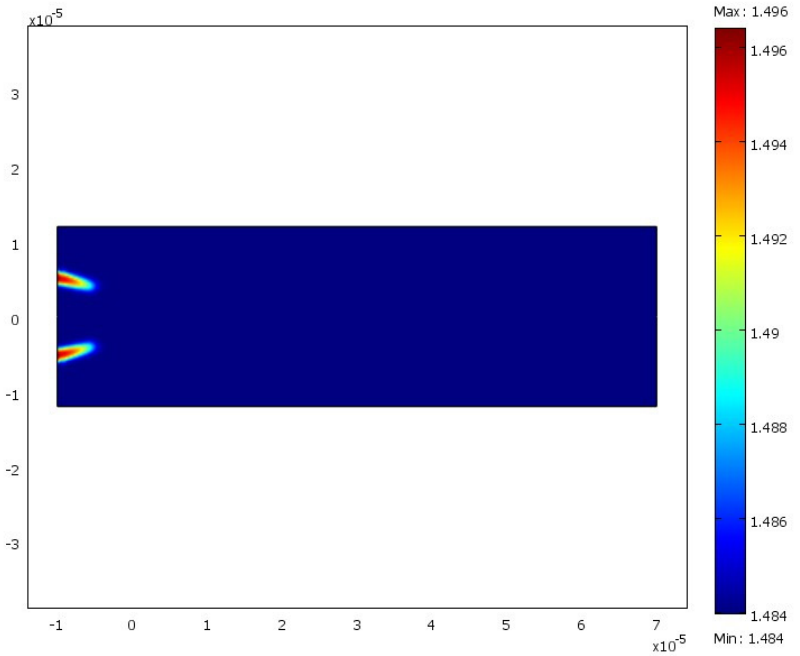
x10-5
3
2
1
0
-1
-2
-3
-1
0
1
2
3
4
5
6
7
x10-5
Max: 1.496
1.496
1.494
1.492
1.49
1.488
1.486
1.484
Min: 1.484

(a) 2 s

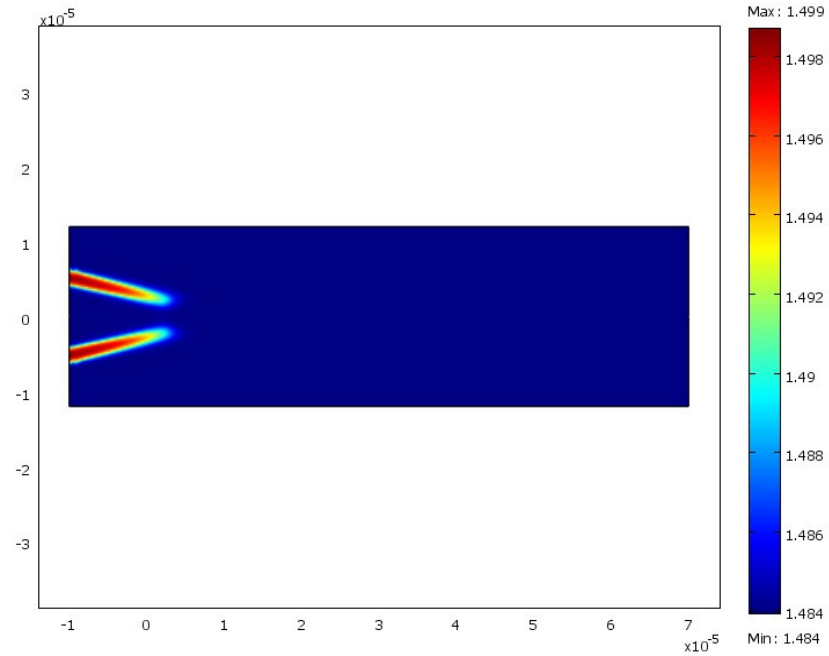
x10-5
3
2
1
0
-1
-2
-3
-1
0
1
2
3
4
5
6
7
x10-5
Max: 1.499
1.498
1.496
1.494
1.492
1.49
1.488
1.486
1.484
Min: 1.484

(b) 5 s

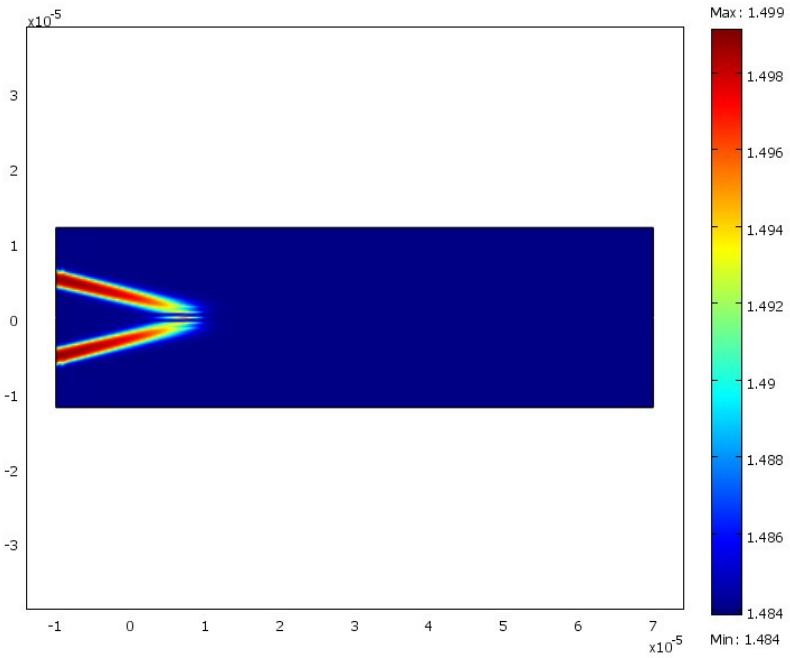
x10-5
3
2
1
0
-1
-2
-3
-1
0
1
2
3
4
5
6
7
x10-5
Max: 1.499
1.498
1.496
1.494
1.492
1.49
1.488
1.486
1.484
Min: 1.484

(c) 7 s

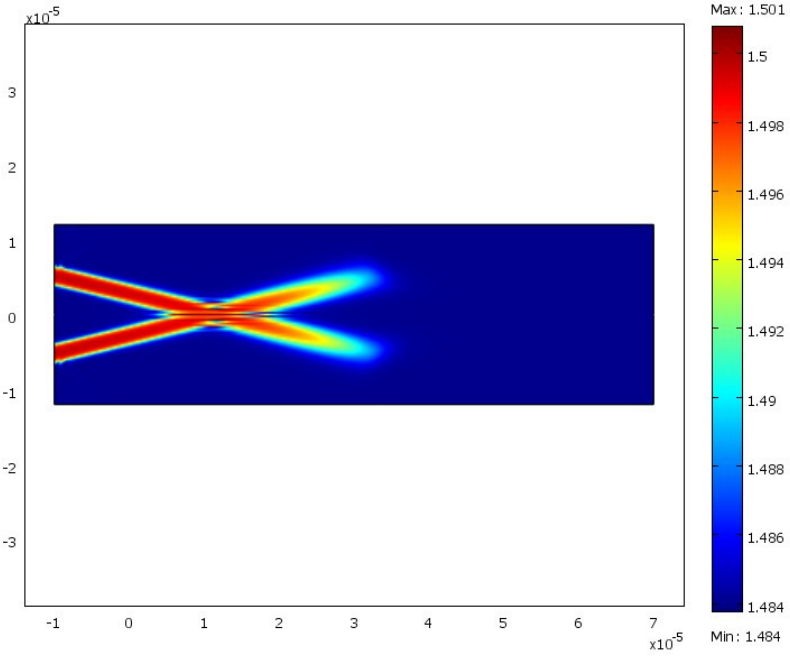
x10-5
3
2
1
0
-1
-2
-3
-1
0
1
2
3
4
5
6
7
x10-5
Max: 1.501
1.5
1.498
1.496
1.494
1.492
1.49
1.488
1.486
1.484
Min: 1.484

(d) 16 s

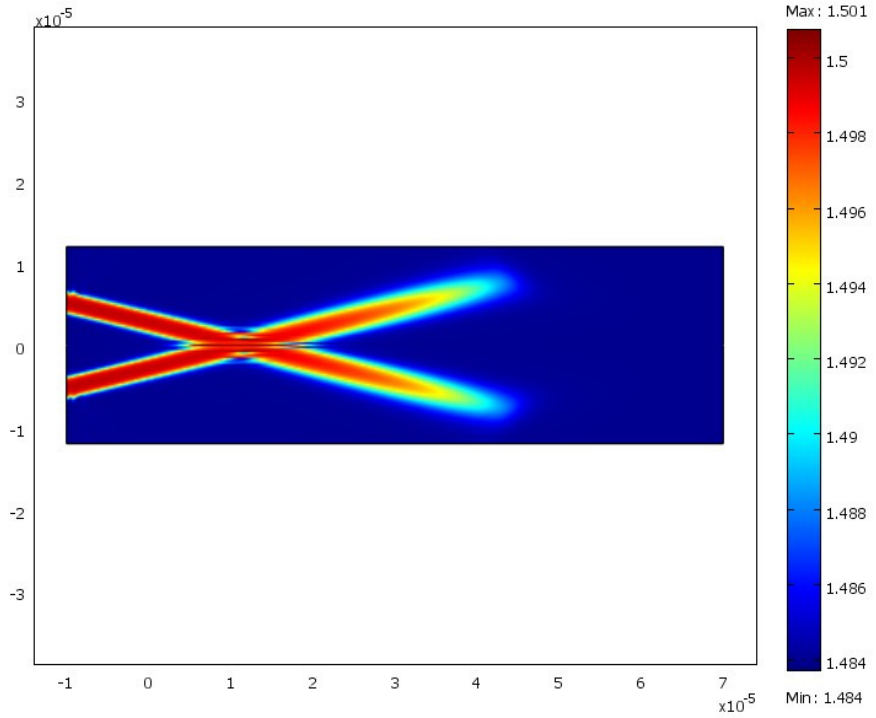
x10-5
3
2
1
0
-1
-2
-3
-1
0
1
2
3
4
5
6
7
x10-5
Max: 1.501
1.5
1.498
1.496
1.494
1.492
1.49
1.488
1.486
1.484
Min: 1.484

(e) 20 s

4.1.2 Waveguides at 17º input angle to the horizontal

The arrival angle of each beam was then reduced to 17° as compared to the horizontal axis. It can be seen from Figure 4.4 that the two waveguides essentially behave in the same way as they do when the input angle is 30º. Only the refractive index distribution for the final time step is presented. One observation that can be made is that the zone of interaction spreads out to some extent in the horizontal direction as compared to the 30º input angle condition.

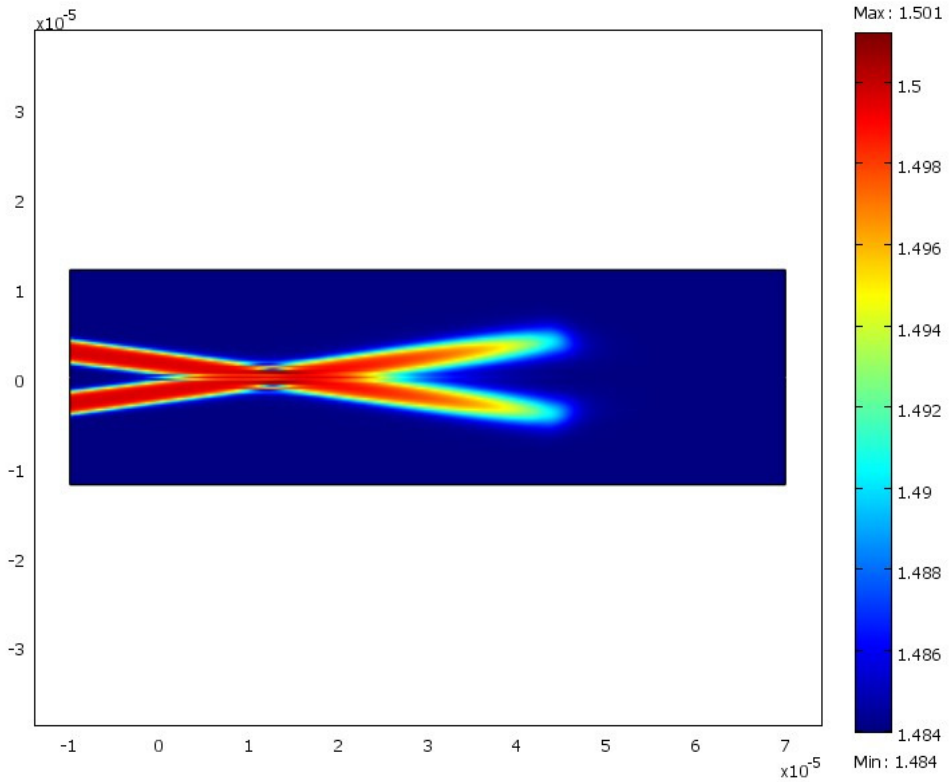

Figure 4.4 Refractive index surface plot for the final step for 17º input angle.

4.1.3 Waveguides at 15º input angle to the horizontal

The arrival angle of each beam was then reduced to 15° as compared to the horizontal axis. It is observed in Figure 4.5 that a third waveguide, although very low in width, is formed along the direction bisecting the angle between the two beams. Also, the zone of interaction spreads out more as compared to the previous result. The third waveguide does appear to be stable and would most likely continue to propagate in a longer time simulation. It is not known if this third waveguide would physically appear in an actual experiment.

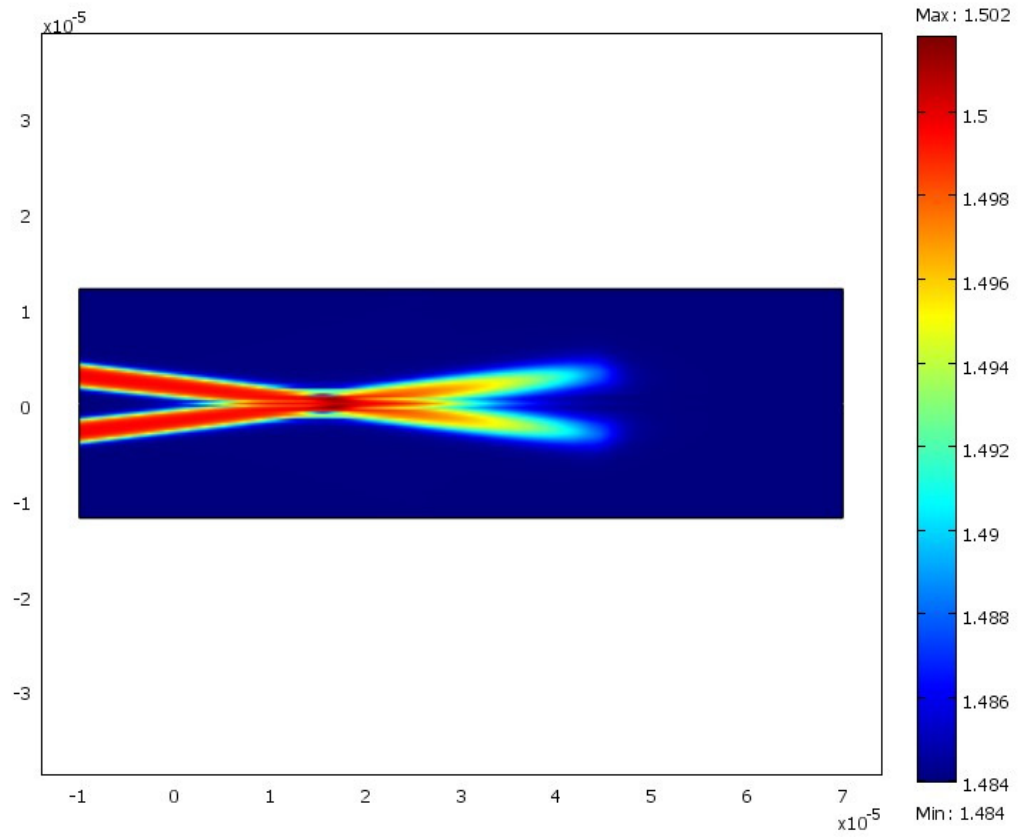

Figure 4.5 Refractive index surface plot for the final step for 15º input angle.

4.1.4 Waveguides at 12º input angle to the horizontal

The relative angle of approach of the two waveguides was further reduced to 12° to the horizontal axis. It can be seen from Figure 4.6 that the third waveguide formed along the horizontal direction became more prominent as compared to the previous, higher angles and starts to saturate. The waveguides on the sides of this central waveguide saturate the same in almost the same manner as the parent waveguides.

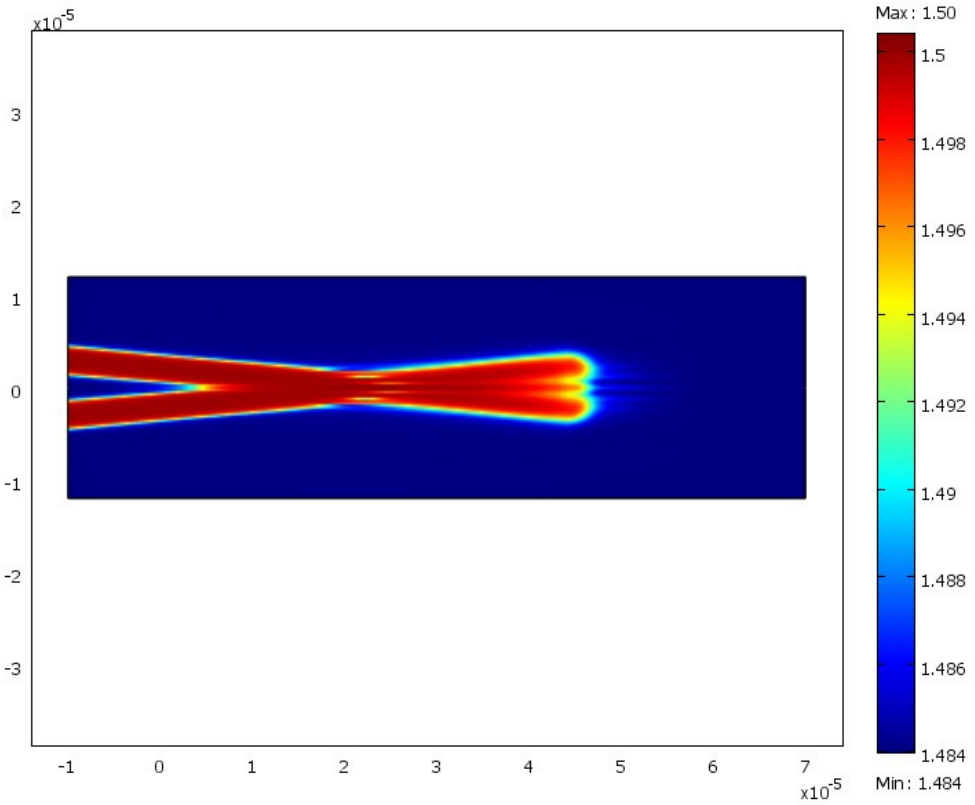

Figure 4.6 Refractive index surface plot for the final step for 12º input angle.

4.1.5 Waveguides at 9º input angle to the horizontal

The relative angle of approach of the two waveguides was further reduced to 9° to the horizontal axis. It can be noticed in Figure 4.7 that the third waveguide formed along the horizontal direction has approximately the same refractive index than the waveguides adjacent to it. Further, the width of this waveguide is also increased as compared to the previous results for higher angles. The zone of interaction has also spread out to a considerable extent.

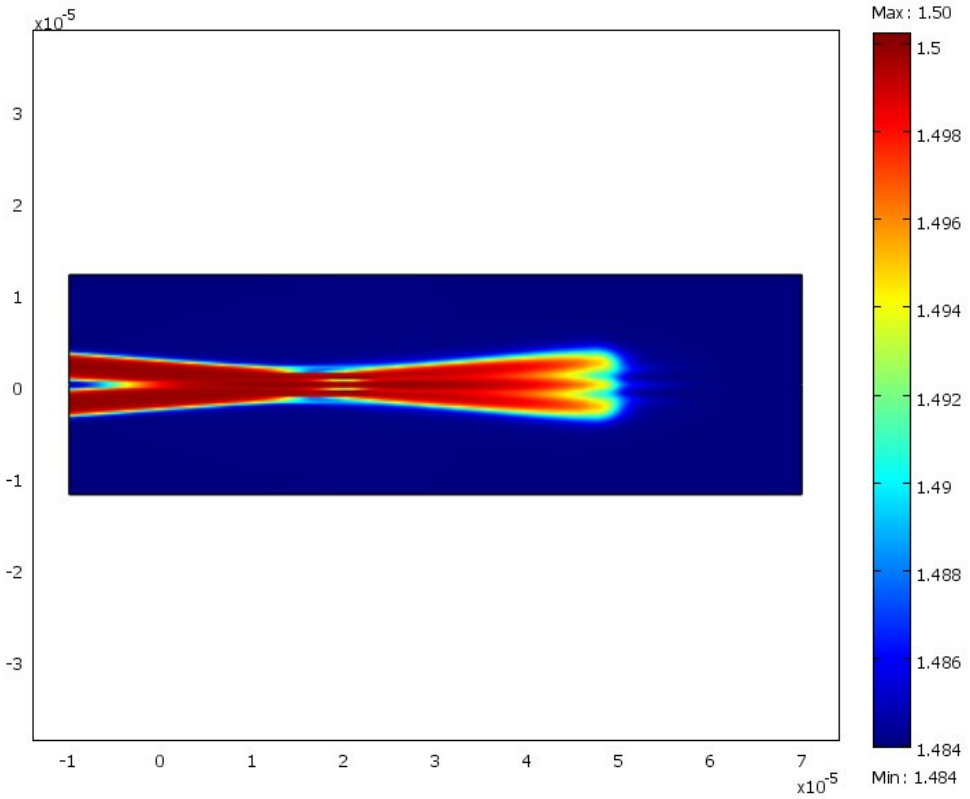

Figure 4.7 Refractive index surface plot for the final step for 9º input angle.

4.1.6 Waveguides at 5º input angle to the horizontal

Finally, the relative angle of approach of the two waveguides was further reduced to 5° to the horizontal axis. It can be seen in Figure 4.8 that the waveguide in the horizontal direction saturates completely whereas the waveguides above and below this waveguide do not saturate and are weaker. The two parent waveguides merge to form a waveguide which propagates along the direction which bisects the angle between the two parent waveguides.

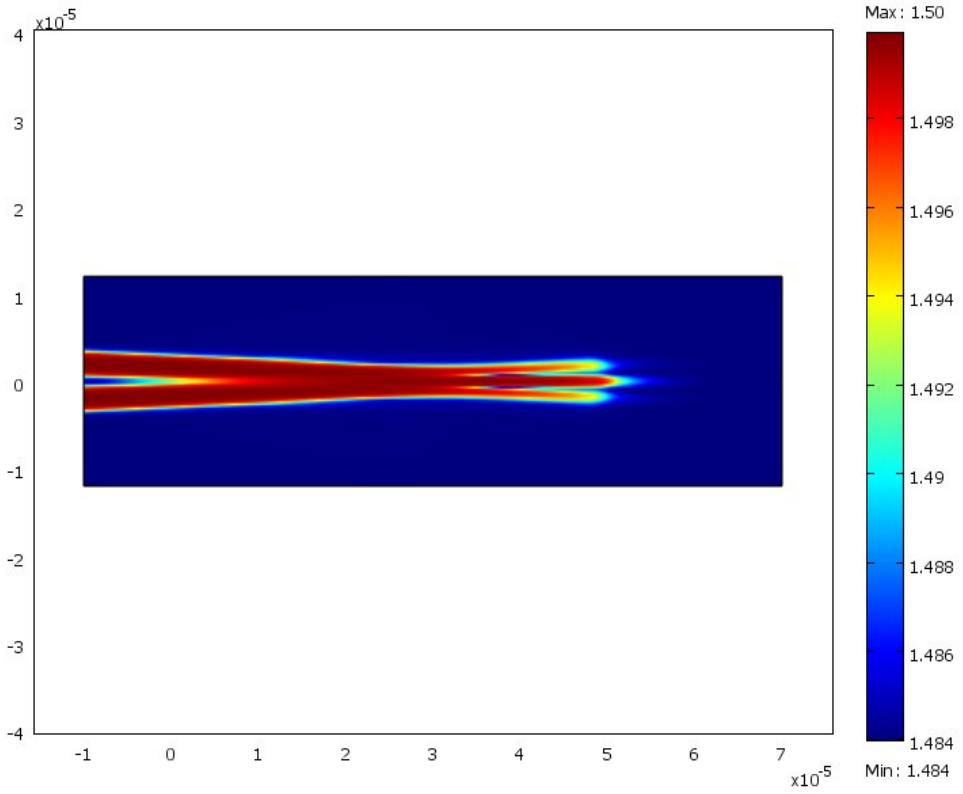

Figure 4.8 Refractive index surface plot for the final step for 5º input angle.

4.1.7 Waveguides at 9º input angle but with the upper beam having half the power of the lower beam

Figures (a)-(f) in the next figure show the refractive index profile for two waveguides arriving at 9° but with the upper beam having half the input power of the lower beam, at selected time steps. It is observed that the lower beam saturates first and forms a wider waveguide as compared to the upper beam, as expected. This is because of the difference in the local intensity that these two beams possess. Further, it is seen that after the interaction between the two waveguides, the waveguide formed propagates in the direction of the beam with higher power which is the lower beam in the case under consideration. Some diffusion of power can be seen propagating in the direction of the original upper beam, however this is much less than the other beam.

Figure 4.9 Refractive index surface plots for input beams with different power inputs. Input angle is 9º for both beams.

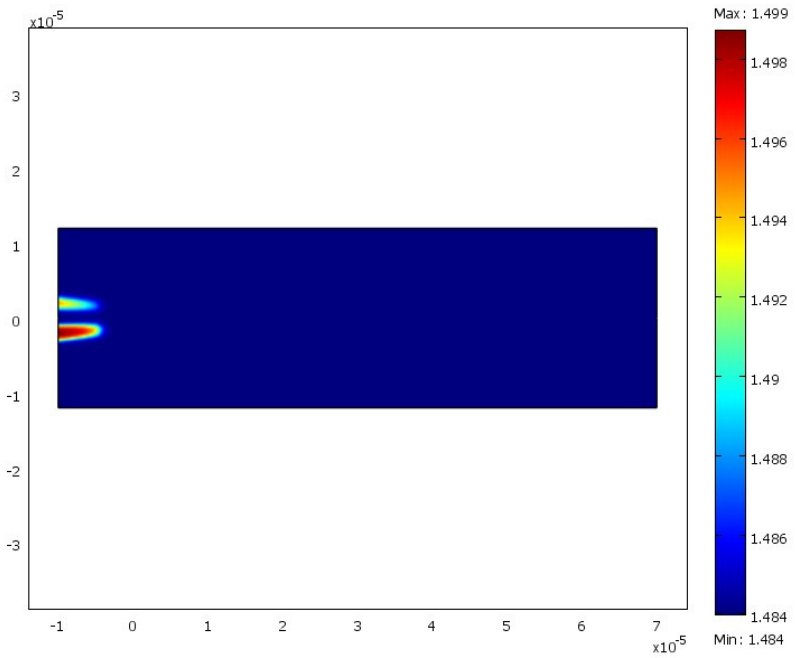
x10-5
3
2
1
0
-1
-2
-3
-1
0
1
2
3
4
5
6
7
x10-5
Max: 1.499
1.498
1.496
1.494
1.492
1.49
1.488
1.486
1.484
Min: 1.484

(a) 2 s

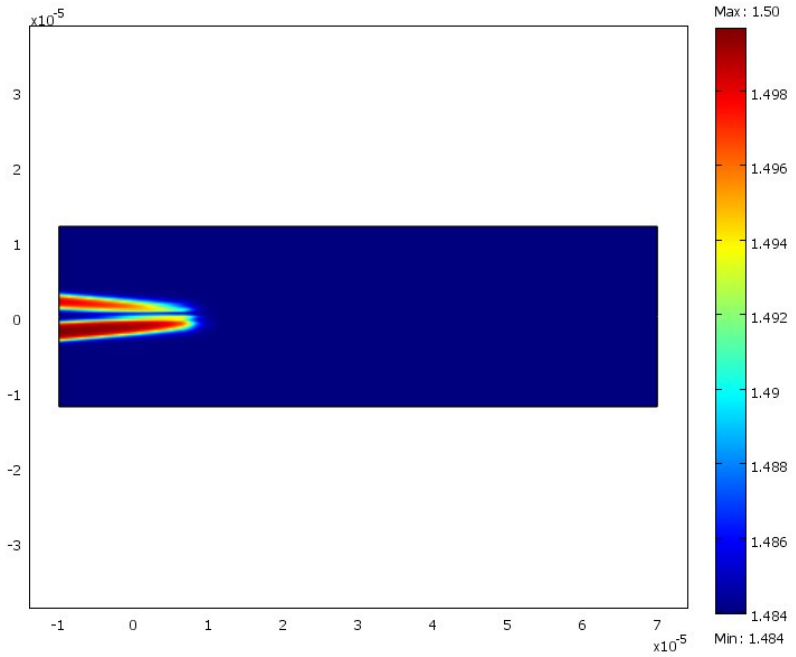
x10-5
3
2
1
0
-1
-2
-3
-1
0
1
2
3
4
5
6
7
x10-5
Max: 1.50
1.498
1.496
1.494
1.492
1.49
1.488
1.486
1.484
Min: 1.484

(b) 6 s

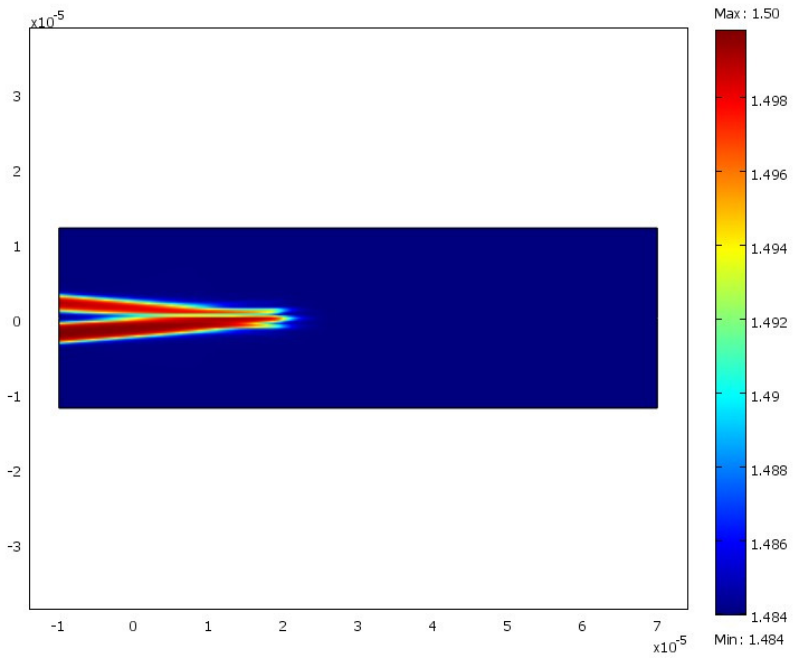
x10-5
3
2
1
0
-1
-2
-3
-1
0
1
2
3
4
5
6
7
x10-5
Max: 1.50
1.498
1.496
1.494
1.492
1.49
1.488
1.486
1.484
Min: 1.484

(c) 10 s

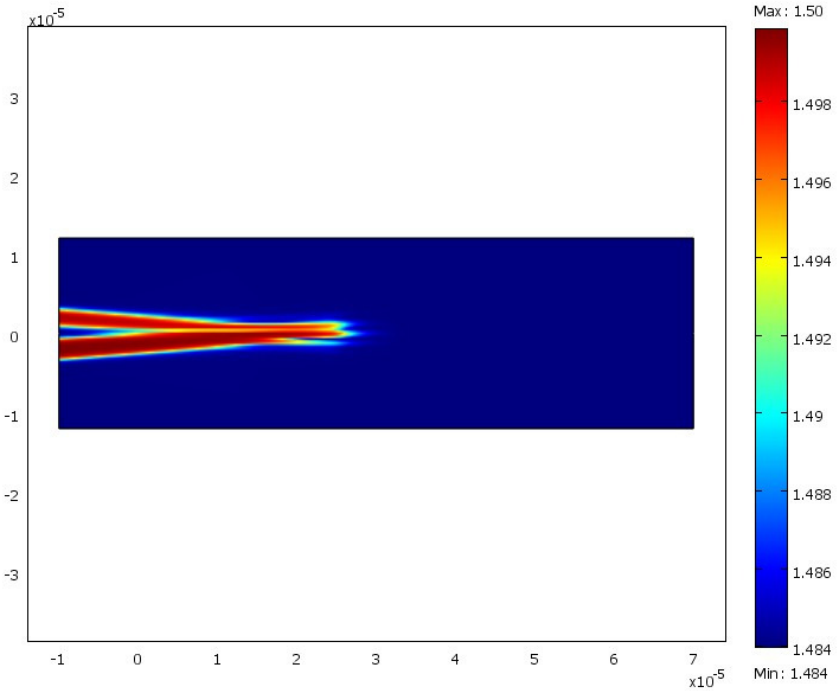
x10-5
3
2
1
0
-1
-2
-3
-1
0
1
2
3
4
5
6
7
x10-5
Max: 1.50
1.498
1.496
1.494
1.492
1.49
1.488
1.486
1.484
Min: 1.484

(d) 12 s

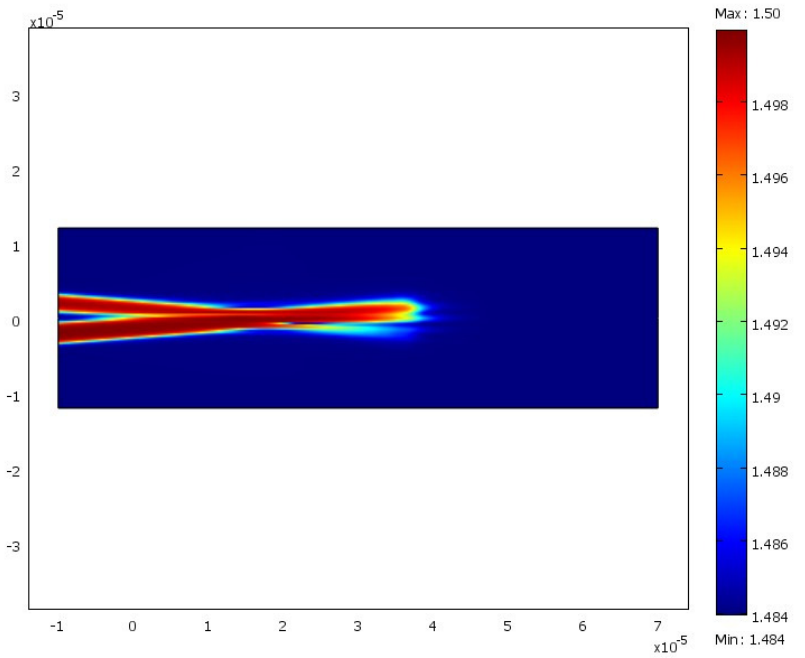
x10-5
3
2
1
0
-1
-2
-3
-1
0
1
2
3
4
5
6
7
x10-5
Max: 1.50
1.498
1.496
1.494
1.492
1.49
1.488
1.486
1.484
Min: 1.484

(e) 16 s

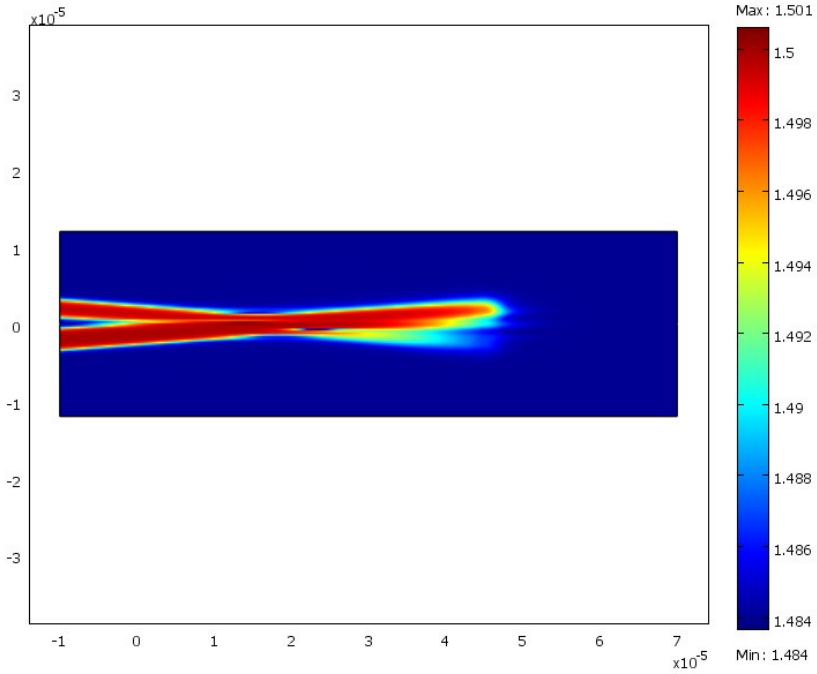
x10-5
3
2
1
0
-1
-2
-3
-1
0
1
2
3
4
5
6
7
x10-5
Max: 1.501
1.5
1.498
1.496
1.494
1.492
1.49
1.488
1.486
1.484
Min: 1.484

(f) 20 s

4.2 Interactions between a polymer element present in the resin and a self-writing waveguide along the horizontal direction

In order to study these interactions, we modeled two types of polymer elements namely, one with approximately the same diameter as the waveguide (thick) and one smaller than the waveguide (thin). For the thick element we modeled the interaction with the element being placed at angles of 10º and 40º relative to the horizontal axis. Two features are different in these simulations than in the previous set. First, the interior boundaries of the domain were drawn for the sake of creating a mapped mesh. These will appear in the result images. A field continuity boundary condition was applied at these boundaries on the propagating electromagnetic waves. The same number of meshed elements were used on each side of the continuity boundaries to prevent numerically generated errors. The second difference is that the 'best case' scenarios have been modeled in this section as the polymer element surface roughness has not been taken into account. In terms of boundary conditions, a scattering boundary condition was applied at the interface between the polymer element and the resin bath, which imposes that there are no reflections from the surface of the polymer element. In reality this would not be the case for a polymer element that was broken from a previous sensor, however we can first understand the best case scenario from these simulations.

4.2.1 Thick polymer element at 10º angle to horizontal

It can be seen from figures (a)-(c) in Figure 4.10 that as the waveguide approaches the polymer element, the normal shape of the self-written waveguide is maintained. Once the waveguide reaches the polymer element no reflections are seen from the surface, as discussed above. The waveguide propagates through to the other side of the polymer element as shown in (d)-(f) and is deflected slightly away from the horizontal and diffracts to some extent due to the interaction between the waveguide and the polymer element. The resulting waveguide is still confined well enough to work as a polymer optical fiber for short distances.

Figure 4.10 Refractive index surface plot for interaction between a thick polymer element at 10º to the horizontal direction and a waveguide.

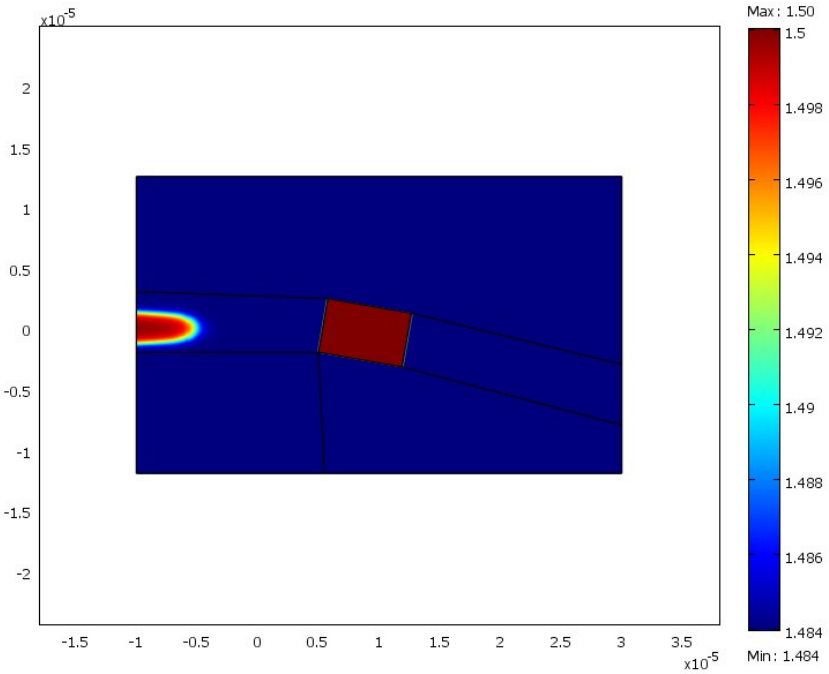
x10-5
2
1.5
1
0.5
0
-0.5
-1
-1.5
-2
-1.5
-1
-0.5
0
0.5
1
1.5
2
2.5
3
3.5
x10-5
Max: 1.50
1.5
1.498
1.496
1.494
1.492
1.49
1.488
1.486
1.484
Min: 1.484

(a) 2 s

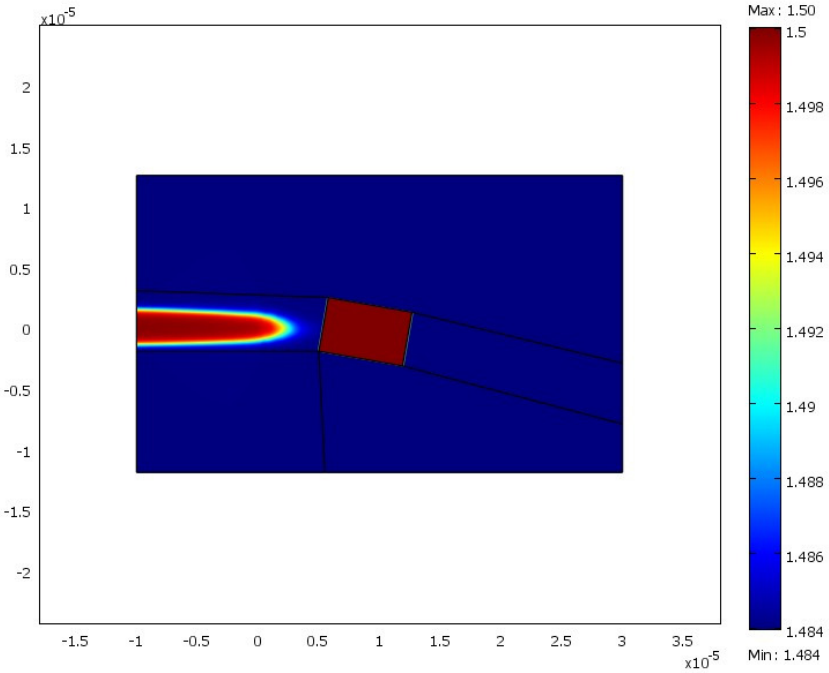
x10-5
2
1.5
1
0.5
0
-0.5
-1
-1.5
-2
-1.5
-1
-0.5
0
0.5
1
1.5
2
2.5
3
3.5
x10-5
Max: 1.50
1.5
1.498
1.496
1.494
1.492
1.49
1.488
1.486
1.484
Min: 1.484

(b) 5 s

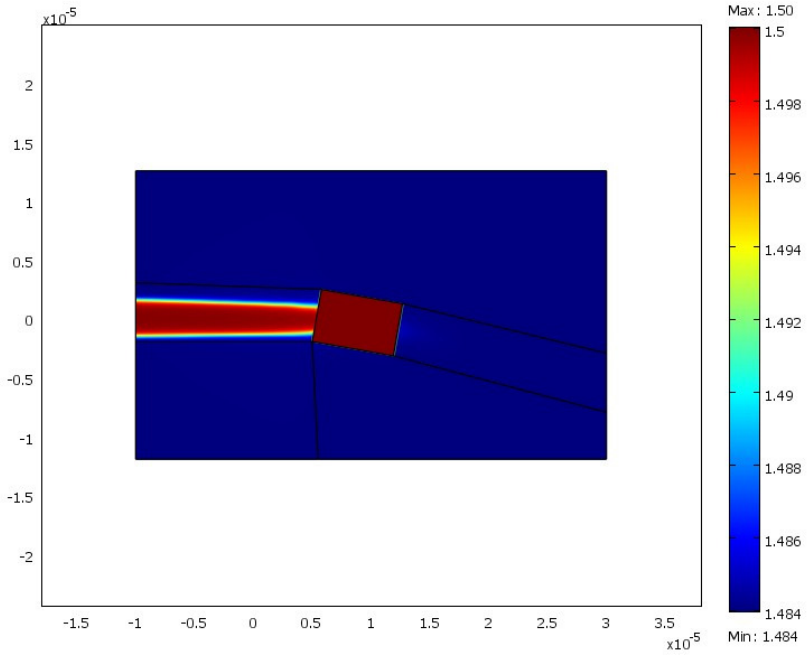
x10-5
2
1.5
1
0.5
0
-0.5
-1
-1.5
-2
-1.5 -1 -0.5 0 0.5 1 1.5 2 2.5 3 3.5
x10-5
Max: 1.50
1.5
1.498
1.496
1.494
1.492
1.49
1.488
1.486
1.484
Min: 1.484

(c) 8 s

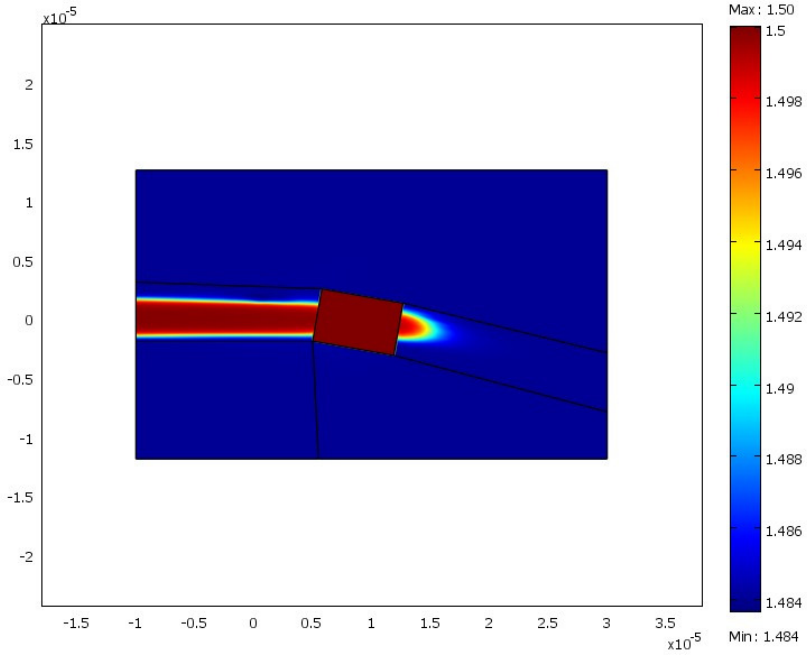
x10-5
2
1.5
1
0.5
0
-0.5
-1
-1.5
-2
-1.5 -1 -0.5 0 0.5 1 1.5 2 2.5 3 3.5
x10-5
Max: 1.50
1.5
1.498
1.496
1.494
1.492
1.49
1.488
1.486
1.484
Min: 1.484

(d) 10 s

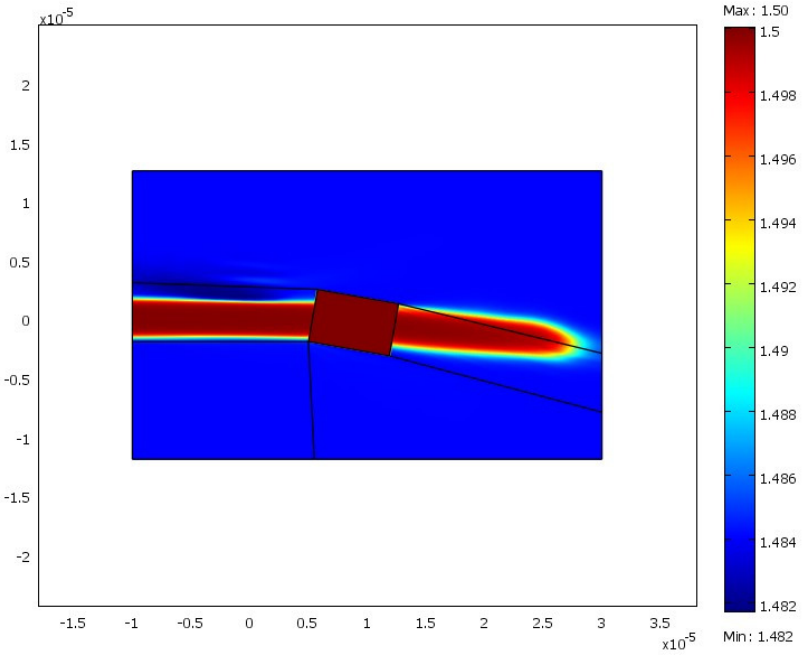
x10-5
2
1.5
1
0.5
0
-0.5
-1
-1.5
-2
-1.5 -1 -0.5 0 0.5 1 1.5 2 2.5 3 3.5
x10-5
Max: 1.50
1.5
1.498
1.496
1.494
1.492
1.49
1.488
1.486
1.484
1.482
Min: 1.482

(e) 15 s

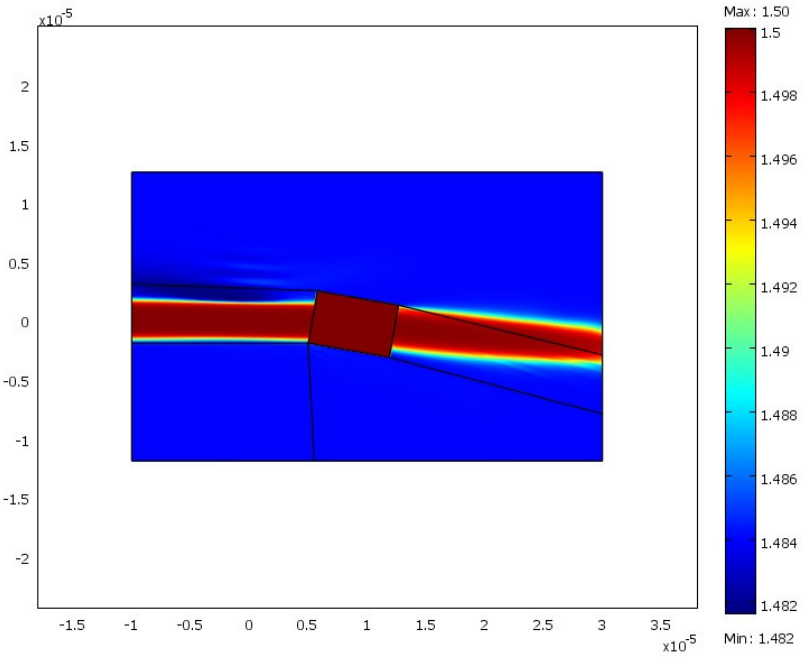
x10-5
2
1.5
1
0.5
0
-0.5
-1
-1.5
-2
-1.5 -1 -0.5 0 0.5 1 1.5 2 2.5 3 3.5
x10-5
Max: 1.50
1.5
1.498
1.496
1.494
1.492
1.49
1.488
1.486
1.484
1.482
Min: 1.482

(f) 20 s

4.2.2 Thick polymer element at 40º angle to horizontal

It can be seen from figures (a)-(d) in Figure 4.11that the behavior of the waveguide in the vicinity of the polymer element before interacting with it is the same as that for the previous case of element at a lower angle. But as seen from figures (e) and (f) in Figure 4.11, the waveguide is distorted slightly near the element and the region of refractive index gradient becomes larger as compared to the previous case. Some of this distortion is due to the fact that the lightwave front intersects the polymer element on two separate faces (see Figure 4.11 (e)) and therefore the angle change in propagation axis is different through the beam. The final waveguide does remain confined after crossing through the polymer element.

Figure 4.11 Refractive index surface plot for interaction between a thick polymer element at 40º to the horizontal direction and a waveguide.

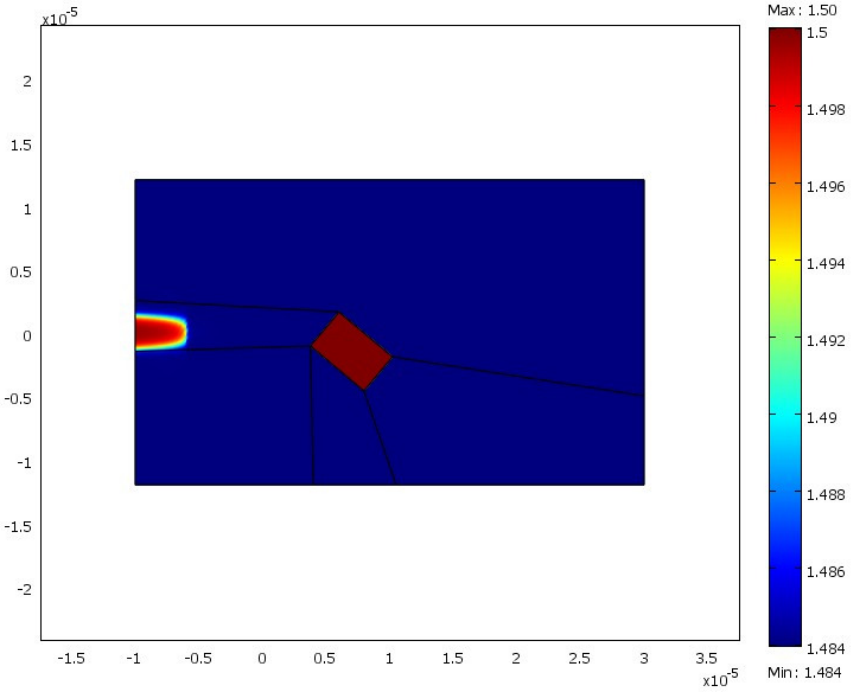
x10-5
2
1.5
1
0.5
0
-0.5
-1
-1.5
-2
-1.5 -1 -0.5 0 0.5 1 1.5 2 2.5 3 3.5
x10-5
Max: 1.50
1.5
1.498
1.496
1.494
1.492
1.49
1.488
1.486
1.484
Min: 1.484

(a) 2 s

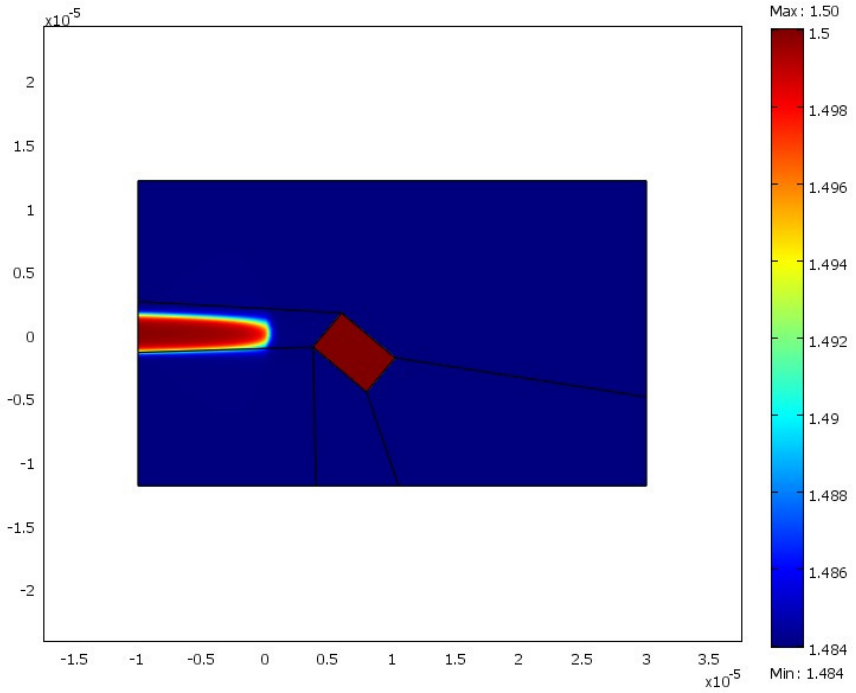
x10-5
2
1.5
1
0.5
0
-0.5
-1
-1.5
-2
-1.5 -1 -0.5 0 0.5 1 1.5 2 2.5 3 3.5
x10-5
Max: 1.50
1.5
1.498
1.496
1.494
1.492
1.49
1.488
1.486
1.484
Min: 1.484

(b) 5 s

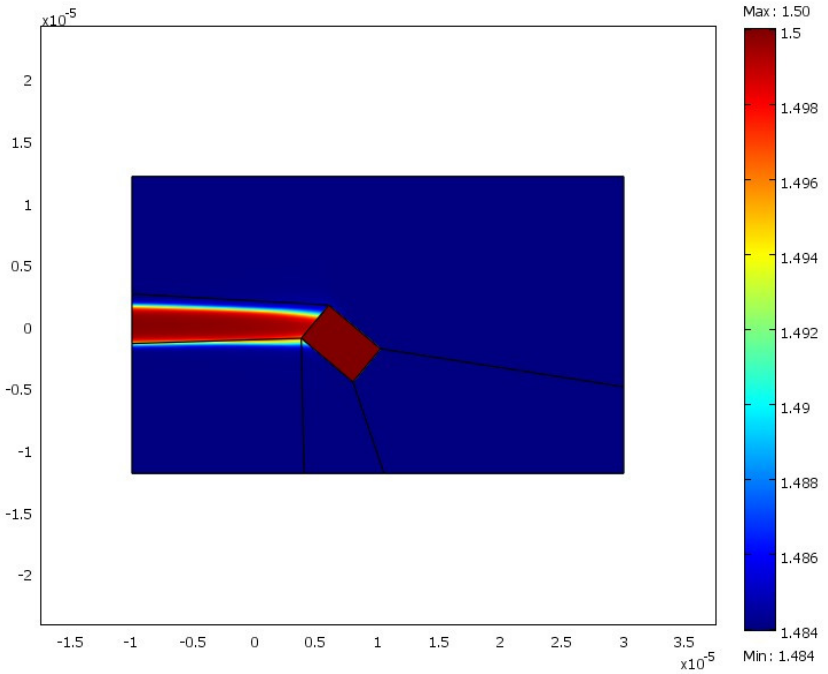
x10-5
2
1.5
1
0.5
0
-0.5
-1
-1.5
-2
-1.5
-1
-0.5
0
0.5
1
1.5
2
2.5
3
3.5
x10-5
Max: 1.50
1.5
1.498
1.496
1.494
1.492
1.49
1.488
1.486
1.484
Min: 1.484

(c) 8 s

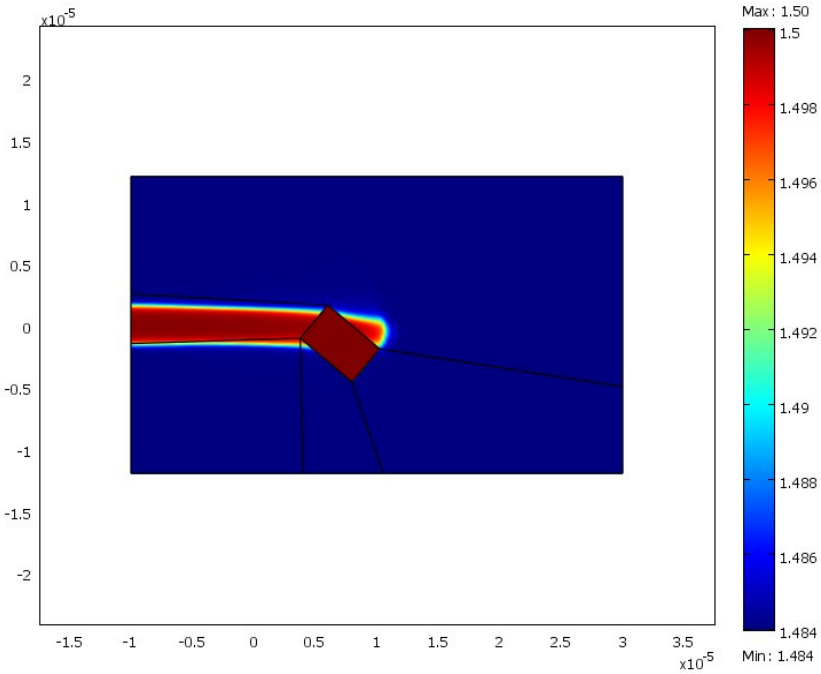
x10-5
2
1.5
1
0.5
0
-0.5
-1
-1.5
-2
-1.5
-1
-0.5
0
0.5
1
1.5
2
2.5
3
3.5
x10-5
Max: 1.50
1.5
1.498
1.496
1.494
1.492
1.49
1.488
1.486
1.484
Min: 1.484

(d) 10 s

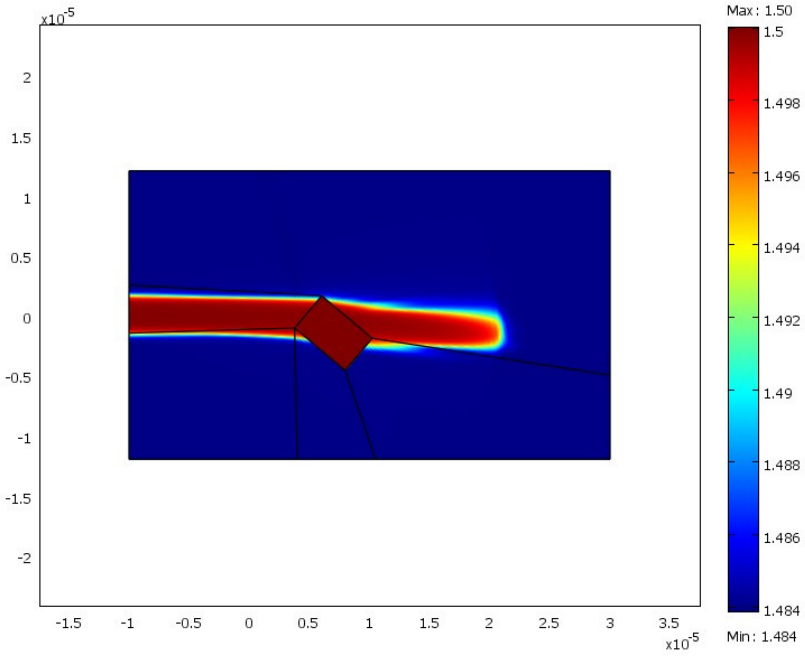
x10-5
2
1.5
1
0.5
0
-0.5
-1
-1.5
-2
-1.5
-1
-0.5
0
0.5
1
1.5
2
2.5
3
3.5
x10-5
Max: 1.50
1.5
1.498
1.496
1.494
1.492
1.49
1.488
1.486
1.484
Min: 1.484

(e) 15 s

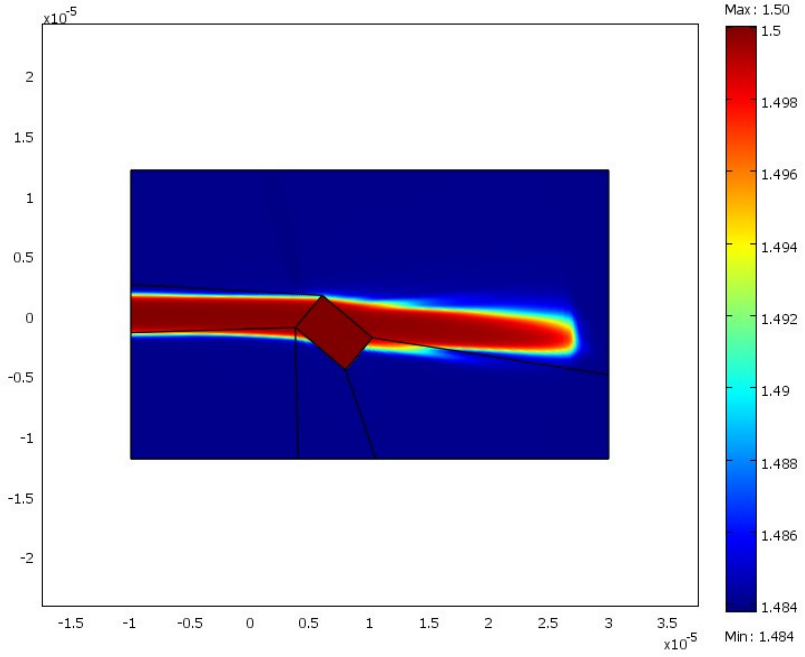
x10-5
2
1.5
1
0.5
0
-0.5
-1
-1.5
-2
-1.5
-1
-0.5
0
0.5
1
1.5
2
2.5
3
3.5
x10-5
Max: 1.50
1.5
1.498
1.496
1.494
1.492
1.49
1.488
1.486
1.484
Min: 1.484

(f) 20 s

4.2.3 Thin polymer element at an angle of 10º to the horizontal

From figures (a)-(c) in Figure 4.12, we observe that the width of the waveguide decreases to match the width of the element but from figures (d) and (e) it can be seen that after propagating a short distance the waveguide distorts and becomes unsymmetric. It is not clear if the waveguide will remained confined in a longer simulation, however losses in the propagating lightwave can be expected. The waveguide prior to arriving at the polymer element appears to be smaller than the previous simulations, however this is because the final time step is only at 12 s.

Figure 4.12 Refractive index surface plot for interaction between a thin polymer element at 10º to the horizontal direction and a waveguide.

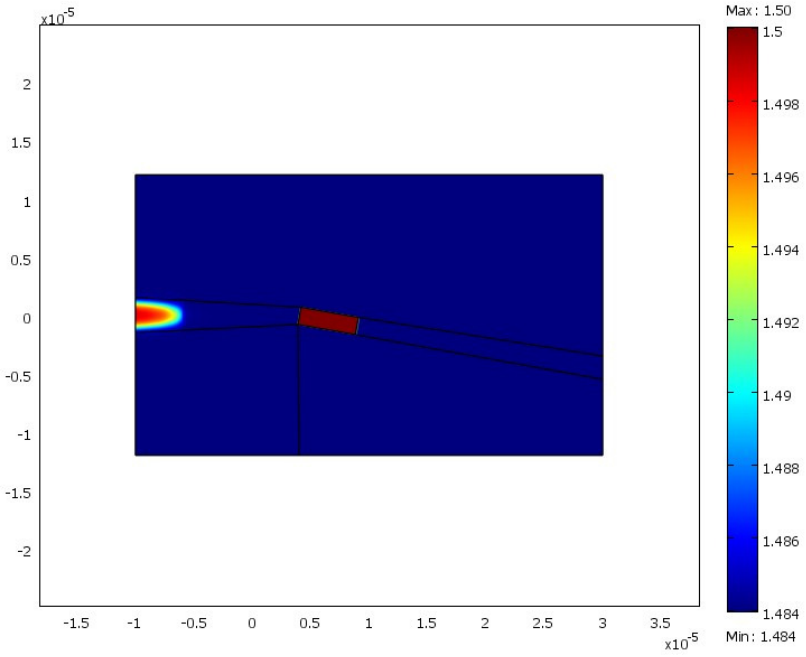
x10-5
2
1.5
1
0.5
0
-0.5
-1
-1.5
-2
-1.5 -1 -0.5 0 0.5 1 1.5 2 2.5 3 3.5
x10-5
Max: 1.50
1.5
1.498
1.496
1.494
1.492
1.49
1.488
1.486
1.484
Min: 1.484

(a) 2 s

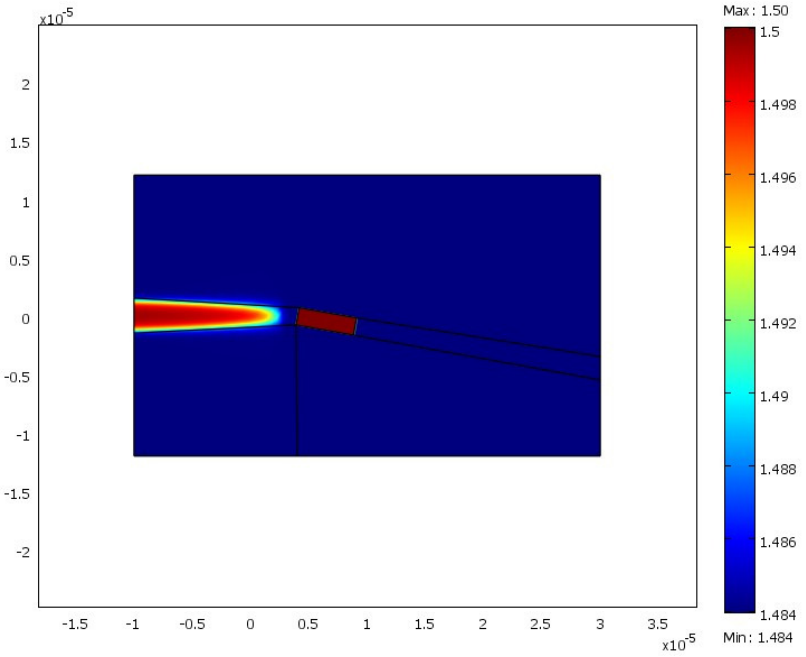
x10-5
2
1.5
1
0.5
0
-0.5
-1
-1.5
-2
-1.5 -1 -0.5 0 0.5 1 1.5 2 2.5 3 3.5
x10-5
Max: 1.50
1.5
1.498
1.496
1.494
1.492
1.49
1.488
1.486
1.484
Min: 1.484

(b) 6 s

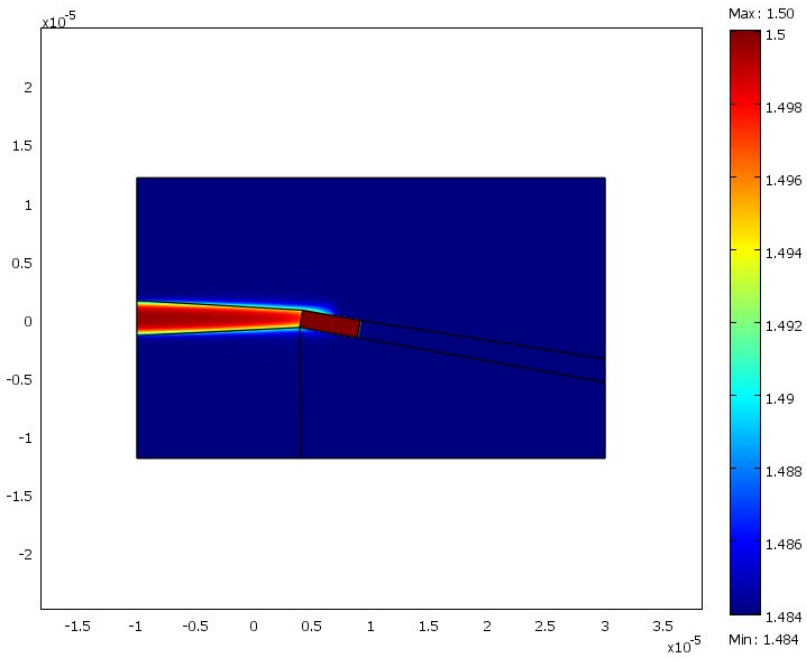
x10-5
2
1.5
1
0.5
0
-0.5
-1
-1.5
-2
-1.5 -1 -0.5 0 0.5 1 1.5 2 2.5 3 3.5
x10-5
Max: 1.50
1.5
1.498
1.496
1.494
1.492
1.49
1.488
1.486
1.484
Min: 1.484

(c) 8 s

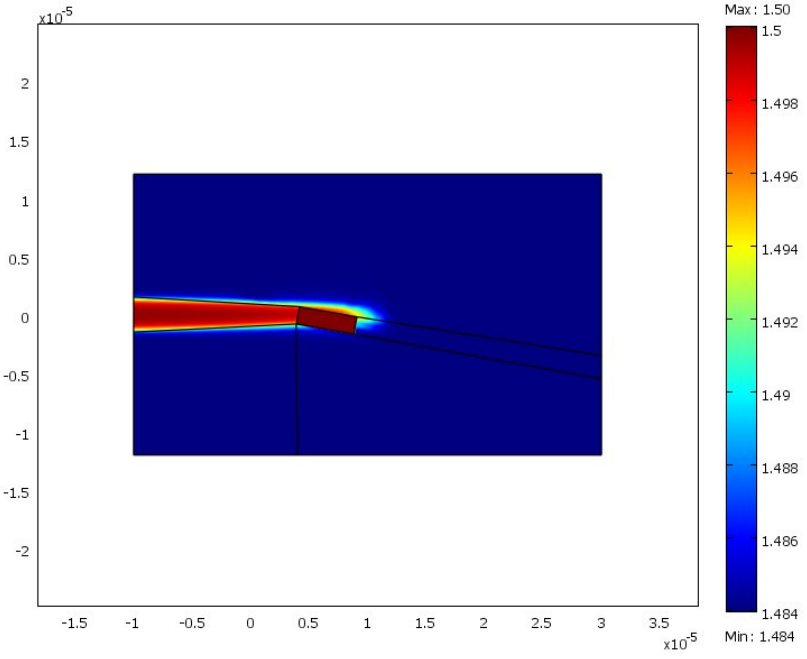
x10-5
2
1.5
1
0.5
0
-0.5
-1
-1.5
-2
-1.5 -1 -0.5 0 0.5 1 1.5 2 2.5 3 3.5
x10-5
Max: 1.50
1.5
1.498
1.496
1.494
1.492
1.49
1.488
1.486
1.484
Min: 1.484

(d) 10 s

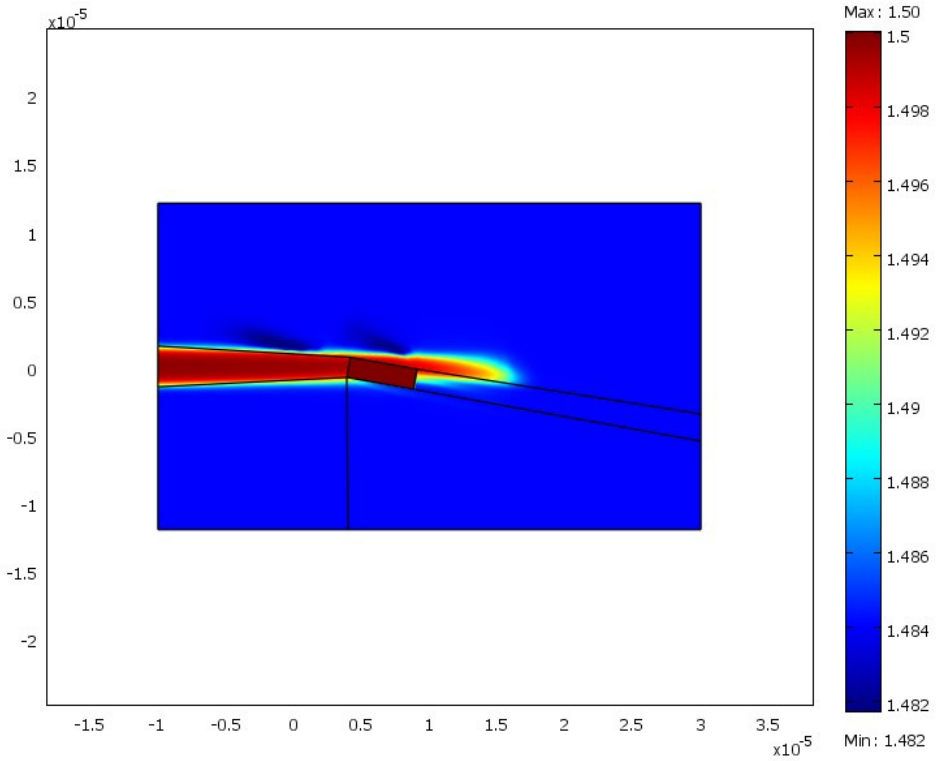
x10-5
2
1.5
1
0.5
0
-0.5
-1
-1.5
-2
-1.5
-1
-0.5
0
0.5
1
1.5
2
2.5
3
3.5
x10-5
Max : 1.50
1.5
1.498
1.496
1.494
1.492
1.49
1.488
1.486
1.484
1.482
Min : 1.482

(e) 12 s

4.3 Discussion

The interactions of solitons or self trapped beams were observed by [11] and [16]. Shoji *et al.* [1] further experimentally studied the interactions of waveguides written by laser beams in a photopolymerizable resin and found out that they behave the same way as solitons. The current research is aimed at recreating these interactions between self-written waveguides in a UV-curable resin using the finite element method. The phenomena of waveguide crossing and merging as experimentally observed by [1] have been demonstrated numerically in this research.

The saturation model described in 3.3 was incorporated in COMSOL in order to simulate the photopolymerization process. For the input angle of 30º , crossing of the two interacting waveguides was observed. It was found by [1] that the two waveguides just pass each other and continue following their respective paths if the angle of collision (this angle is measured between the horizontal axis and the propagation axis of the beam) is greater than the critical angle. Hence it can be said that the angle of 30º is greater than the critical angle. As the angle was decreased to 17º, similar effects were observed which means that this angle is still greater than the critical angle. When the collision angle is further reduced to 15º as shown in Figure 4.5, a very thin waveguide appears along the direction which bisects the angle between the two interacting waveguides in addition to the propagating waveguides after interaction. From further simulations, as shown in Figure 4.6, Figure 4.7 and Figure 4.8 for collision angles of 12º, 9º and 5º respectively, strengthening of the central waveguide was observed. Eventually, the central waveguide was more dominant as compared to the adjacent waveguides after interaction of the parent waveguides coming into the domain from left boundary.

From these simulations, we can deduce that the critical angle is approximately 15º as the central waveguide first appears at this angle for all the angles that have been considered in this research. These observations seem to be in agreement with the observations made by [1] in their experimental setup although the resin systems are not the same. Another observation that they made was that if the power of the two input beams are different, the waveguide formed after the interaction of the two waveguides written by these beams propagates in the direction of the beam with higher power. From the current research, the propagation of the effective waveguide was in the direction of the lower beam when modeled with the finite element simulation.

Generally the collision scenarios are therefore in good accord with the observations made by [1].

The details of the interaction region between the two waveguides are not as well predicted by the current simulations. In particular, for collision angles below the critical angle,three waveguide branches were predicted after the collision. In the previous experiments, only the central waveguide was observed. While, this central waveguide was strengthened as the collision angle decreased, a significant portion of the lightwave energy continued in the original direction of the input lightwaves (as can be observed by the fact polymerization occurred along these directions). These are similar issues to that of the numerical simulations of [11]. It is also likely that the reasons for these discrepancies are the same of the simulations of [11]. One of the fundamental assumptions of the solution (by reducing the time scale of the photopolymerization to that of the lightwave propagation) is that the index of refraction changes are quasi-static as compared to the lightwave propagation. This assumption is less valid at the point where the waveguides interact. A second potential source of error is the fact that the finite model presents a perfect system. In other words, while the additional two waveguide branches may not be stable there are no imperfections in the finite element model to cause them to dissipate.

A second kind of interaction between a polymer element already present in the UV-curable resin and a self-written waveguide were simulated for the ideal case, that is, without any surface roughness for the polymer element. These interactions were observed for thick polymer element (the element width is greater than the width of the written waveguide) inclined at shallow and steep angles to the horizontal. Similar interaction was observed for a thin element (the element width is smaller than the width of the written waveguide) inclined at an angle of 10º to the horizontal axis. For the angle of 10º, it was observed that the waveguide slightly deflects downwards as compared to the horizontal direction but is uniform enough to be considered as a polymer optical fiber. The width of the propagating waveguide after the interaction remains almost the same as before the interaction. Further, the angle of the polymer element was increased to 40º as shown in Figure 4.11 and it was observed that the waveguide after interaction with the element is distorted near the element and the region of refractive index gradient spreads out more as compared to the previous case of 10º. In addition to these simulations, a thin polymer element was placed in the resin at angle of 10º to the horizontal and a waveguide was

made to interact with it. From Figure 4.12 it was observed that the width of the polymer element was less than that of the waveguide interacting with it. The refractive index slightly increased around the element but eventually the waveguide weakens after it propagates further ahead of the element. This simulation demonstrates that the polymer element could significantly distort a waveguide crossing the element. Also, the surface roughness of the element should be incorporated into the model to better understand this phenomenon.

Finally, one known effect that was not incorporated in this code was the mechanical shrinkage due to the change in density of the resin as the waveguide propagates further into the resin. These effects were observed by [3] for a single waveguide and this would be of interest for the interacting waveguides, although their effect on the final waveguide geometry would be minimal.

Chapter 5 Conclusions and Future Work

5.1 Conclusions

The primary goal of the current research was to recreate the interaction scenarios between two self-written waveguides and between a polymer element and a self-written waveguide using a multi-physical finite element model. This thesis has successfully put forward the development of the model that can be modified for different physical situations in order to handle the interactions between waveguides in different photosensitive resins undergoing the photopolymerization process. This model was implemented into the commercial finite element code COMSOL.

In this thesis, the physical aspects of electromagnetics of planar Gaussian beams and the chemistry of the resin polymerization have been coupled in order to simulate the photopolymerization process for the formation of waveguides in the resin. Appropriate boundary conditions were applied to simulate two waveguides propagating into the resin at an angle to the horizontal from the left boundary of the resin bath. The interactions observed by [1] were successfully simulated using this code. Other interesting simulations like the interactions between a polymer element and a waveguide in the resin were carried out using COMSOL.

Further, the use of a commercially available finite element code allows for easier application by many researchers. This model can be said to be adaptable as changing the parameters of the resin and the input conditions can predict different interaction scenarios under different conditions.

5.2 Future Work

The future work proposed for this research would be the application of the model developed in this research to experimentation using several resins with different refractive indices in order to see how the resins react in a laboratory setup. The interactions observed in this research would be recreated for these resins and parameters like the critical angle of the

collision and the time required for achieving saturation and propagation of waveguides in the resins could be evaluated in order to calibrate the resins on the basis of these parameters.

REFERENCES

[1] Andrey A. Sukhorukov, Satoru Shoji and Yuri S. Kivshar, "Self-written waveguides in photosensitive materials", *Journal of Nonlinear Optical Physics* & *Materials*, Vol. 11, No. 4 (2002) 391-407

[2] Yuri S. Kivshar and George I. Stegeman, "Spatial optical solitons-guiding light for future technologies", *Optics and Photonics News*, 2002

[3] Aliesha Anderson and Kara Peters, "Finite element simulation of self-writing waveguide formation through photopolymerization", *Journal of Lightwave Technology*, Vol. 27, No. 24, December 15, 2009

[4] Aliesha Anderson, "Finite element formulation of self-writing of polymer optical fiber sensors", *Master of Science Thesis*, North Carolina State University, 2008

[5] Shoji Maruo, Osamu Nakamura and Satoshi Kawata, "Three dimensional microfabrication with two-photon-absorbed photopolymerization", *Journal of Optical Society of America*, Optics Letters, Vol. 22, No. 2, January 15, 1997

[6] Andrey A. Sukhorukov and Yuri Kivshar, "Self-trapped optical beams: Spatial solitons", *Pramana Journal of Physics*, Vol. 57, Nos 5 & 6, Nov. & Dec. 2001 pp.1079-1096

[7] Andrey A. Sukhorukov, Satoru Shoji and Yuri S. Kivshar, "Self-written waveguides in photopolymerizable resins", Optics Letters, *Journal of Optical Society of America*, February 1, 2002, Vol. 27, No. 3

[8] Manabu Kagami, Tatsuya Yamashita, Masatoshi Yonemura, Akari Kawasaki, Masaaki Tsuchimori and Takayuki Matsui, "Light-induced self-written three-dimensional polymer optical waveguide for module fabrication and interconnection", *Journal of Optical Society of America*, 2006

[9] Heike Ebendroff-Heidepriem, "Laser writing of waveguides in photosensitive glasses", *Elsevier, Optical Materials*, 2003, Optical Materials 25 109-115

[10] Haiying Huang, Ayan Majumdar and Jae-Sung Cho, "Fabrication and evaluation of hybrid silica/polymer optical fiber sensors for large strain measurement", *Transactions of The Institute of Measurement and Control*, 3-4 (2009) pp.247-257

[11] Steffen Kjær Johansen, Ole Bang and Mads Peter Sorensen, "Escape angles in bulk $\chi^{(2)}$ soliton interactions", *Journal of the American Physical Society*, 2002, Physical Review E. Volume 65. 026601

[12] J.P. Gordon, "Interaction forces among solitons in optical fibers", *Journal of Optical Society of America*, Optics Letters, Vol. 8, No. 11, November 1983

[13] Young J. Song, Kara J. Peters, "Self-repairing polymer optical fiber sensor", *Proc. Of SPIE*, Vol. 7648, 2010

[14] Kokou Dorkenoo, Olivier Crégut, Loïc Mager and Fabrice Gillot; Christiane carre, Alain Fort, "Quasi-solitonic behavior of self-written waveguides created by photopolymerization", *Journal of Optical Society of America*, Optics Letters, Vol. 2, No.20, October 15, 2002

[15] K.D. Dorkenoo, F. Gillot, O. Crégut, Y. Sonnefraud, A. Fort and H. Leblond, "Control of refractive index in photopolymerizable materials for (2+1)D solitary waveguide formation", *The American Physical Society*, Physical Review Letters, Vol. 93, No. 14, October 1 2004

[16] Dumitru Mihalache and Dumitru Mazilu, Falk Lederer, Yuri S. Kivshar, "Collisions between discrete surface spatiotemporal solitons in nonlinear waveguide arrays", *The American Physical Society*, Physical Review A 79, 013811, 2009

[17] Yuval P. Shapira and Moshe Horowitz, "Two-soliton interaction in the vicinity of a defect inside a fiber bragg grating and its application for obtaining an all-optical memory, *Journal of Optical Society of America*, Optics Letter, Vol.33 No.7, April 1 2008

[18] Okihiro Sugihara, Shuhei Yasuda, Bin Cai, Kyoji komatsu and Toshikuni Kaino, "Serially grafted polymer optical waveguides fabricated by light-induced self-written

waveguide technique, *Journal of Optical Society of America*, Optics Letters, Vol.33, No.3, February 1 2008

[19] Tanya M. Monro, L. Poladian, C. Martijn de Sterke, "Numerically efficient modal decomposition approach to self-writing processes", *Journal of Optical Society of America*, Vol.14, No.9, September 1997

[20] Tanya M. Monro and Martijn de Sterke, I. Poladian, "Analysis of self-written waveguide experiments", *Journal of Optical Society of America*, Vol.16, No.10, October 1999

[21] Kokou Dorkenoo, A.J. van Wonderen, Hervé Bulou, Michelangelo Romeo, Olivier Crégut and Alain Fort, "Time-resolved measurement of the refractive index of photopolymerization", *American Institute of Physics*, Applied Physics Letters, Volume 83, Number 12, September 22 2003

[22] Yan Zhang and Chun-Fang Li, "On the representation of an inclined Gaussian beam", *European Journal of Physics*, 27, 779-786, 2006

[23] Malik Hocine, Nicolas Fressengeas and Godefroy Kugel; Christiane Carré and Daniel Joseph Lougnot; Renaud Bachelot and Pascal Royer, "Modeling the growth of a polymer microtip on an optical fiber end", *Journal of Optical Society of America*, Vol. 23, No. 4, April 2006